JOURNAL OF GEOPHYSICAL RESEARCH, VOL. 102, NO. D24, PAGES 29,167–29,188, DECEMBER 26, 1997

Case study modeling of turbulent and mesoscale fluxes over the BOREAS region

Pier Luigi Vidale and Roger A. Pielke Sr.
Department of Atmospheric Science, Colorado State University, Fort Collins

Louis T. Steyaert
U.S. Geological Survey, EROS Data Center, NASA Goddard Space Flight Center, Greenbelt, Maryland

Alan Barr
Atmospheric Environment Service, National Hydrology Research Centre, Saskatoon

Abstract. Results from aircraft and surface observations provided evidence for the existence of mesoscale circulations over the Boreal Ecosystem-Atmosphere Study (BOREAS) domain. Using an integrated approach that included the use of analytical modeling, numerical modeling, and data analysis, we have found that there are substantial contributions to the total budgets of heat over the BOREAS domain generated by mesoscale circulations. This effect is largest when the synoptic flow is relatively weak, yet it is present under less favorable conditions, as shown by the case study presented here. While further analysis is warranted to document this effect, the existence of mesoscale flow is not surprising, since it is related to the presence of landscape patches, including lakes, which are of a size on the order of the local Rossby radius and which have spatial differences in maximum sensible heat flux of about 300 W m^{-2}. We have also analyzed the vertical temperature profile simulated in our case study as well as high-resolution soundings and we have found vertical profiles of temperature change above the boundary layer height, which we attribute in part to mesoscale contributions. Our conclusion is that in regions with organized landscapes, such as BOREAS, even with relatively strong synoptic winds, dynamical scaling criteria should be used to assess whether mesoscale effects should be parameterized or explicitly resolved in numerical models of the atmosphere.

1. Introduction

It has long been recognized that land and sea contrasts produce sea breezes [e.g., *Simpson*, 1994]. More recently, it has become evident that landscape variations which result in spatial gradients in surface heat flux can generate mesoscale circulations as strong as sea breezes [e.g., *Ookouchi et al.*, 1984; *Segal et al.*, 1988; *Avissar and Pielke*, 1989; *Segal and Arritt*, 1992; *Chen and Avissar*, 1994; *Cotton and Pielke*, 1995]. However, the minimum horizontal variation in surface heating flux required for the generation of a significant mesoscale circulation has yet to be determined. *Xian and Pielke* [1991] and *Pielke et al.* [1991] addressed this issue in idealized, two-dimensional numerical experiments.

During the last decade or so, procedures to represent landscape heterogeneity within a larger-scale area, such as a general circulation model (GCM) or numerical weather prediction (NWP) grid cell, have focused on a summation of surface fluxes within that area, proportionally weighted by the fluxes from each land surface type. Examples of this approach were reported by *Avissar and Pielke* [1989], *Li and Avissar* [1994], *Kosta and Suarez* [1992], *Bonan et al.* [1993], *Pleim and Xiu* [1995], *Pitman* [1994], *Henderson-Sellers et al.* [1993], *Miller* [1993], *Shen and Arritt* [1996], *Collins and Avissar* [1994], *Clark and Arritt* [1995], and *Sun and Mahrt* [1995]. Mesoscale effects have been ignored in this type of land surface flux representation.

There is convincing modeling evidence, however, that mesoscale fluxes resulting from landscape heterogeneity in flat terrain, averaged over the scale of a GCM or NWP model grid increment, can often be of the same order of magnitude as the turbulent fluxes as well as have a different vertical distribution. Examples of studies that document the modification of atmospheric boundary layer structure and/or the development of mesoscale flow due to land surface inhomogeneity were reported by *Pielke et al.* [1991, 1993], *Dalu et al.* [1991], *Cotton and Pielke* [1995], *Segal and Arritt* [1992], *Avissar and Pielke* [1989], *Manqian and Jinjun* [1993], *Raupach* [1991], *Guo and Schuepp* [1994], *Zhong and Doran* [1995], *Lynn et al.* [1995], *Avissar and Chen* [1993], *Chen and Avissar* [1994], and *André et al.* [1989a]. A number of these papers are summarized by *Cotton and Pielke* [1995]. These mesoscale fluxes have substantial coherent structure and are therefore predictable features [i.e., *Zeng and Pielke*, 1993, 1995a; *Zeng*, 1992]. *Zeng and Pielke* [1995b] concluded that important controls on mesoscale fluxes include planetary boundary layer depth, horizontal size of the surface heat patches, the potential temperature difference between different patches, the surface heat, water, and momentum fluxes, and height above the surface.

Observations have also documented the importance of heterogeneous landscape in influencing boundary layer structures

Paper number 97JD02561.
0148-0227/97/97JD-02561$09.00

and mesoscale fluxes [*Mahrt and Ek*, 1993; *Mahrt et al.*, 1994a, b; *Doran et al.*, 1992, 1995; *Smith et al.*, 1992; *Beljaars and Holtslag*, 1991; *Segal et al.*, 1988, 1989; *Balling*, 1988] and in affecting such related properties as soil water infiltration [*Wood et al.*, 1992].

Therefore there is a need for studies that investigate the potential influence of mesoscale fluxes due to heterogeneous land surface conditions on larger-scale atmospheric structures. *Claussen* [1991], for example, discussed how land surface variability influences spatially averaged fluxes and spatially averaged vertical gradients, although his analysis was limited to the situation where the boundary layer becomes homogeneous above a "blending height," located within the surface layer [*Wierenga*, 1986]; *Mahrt* [1987] and *Mason* [1988] also have papers concerning this topic. Furthermore, *Doran and Zhong* [1995] showed that variability of mixed layer depths over heterogeneous landscape can be significant and can lead to errors in flux parameterizations when ignored. *Wang et al.* [1997] gave an evaluation of the mesoscale flow for a stochastic distribution of thermal inhomogeneities, showing how, by using a three-dimensional, nonlinear numerical model, the impact of synoptic wind on mesoscale circulations is relatively weak, although mesoscale heat fluxes were found to be smaller on days with sustained winds than on days with weak winds. They also showed how the impact of the thermally induced mesoscale circulations can represent a significant heat transport mechanism, extending up to about 5 km when the atmosphere is neutral, although it can become suppressed when the atmosphere is stable. Mesoscale momentum fluxes, on the other hand, were found to be comparable to turbulent momentum fluxes even in a stable atmosphere.

Field programs which focus on land-surface–atmosphere interactions provide an observational database that can be compared with model results. Some examples are FIFE [*Sellers et al.*, 1992; *Betts and Beljaars*, 1993] in Kansas, United States; the Boreal Ecosystem-Atmosphere Study (BOREAS) [*Sellers et al.*, 1995; JGR papers, this issue] in Saskatchewan and Manitoba, Canada; LOTREX [*Schädler et al.*, 1990] in Hildesheimer Börde, Germany; EFEDA [*Bolle et al.*, 1993] in Spain; HAPEX-MOBILHY [*André et al.*, 1989b; *Noilhan et al.*, 1991] in France; HAPEX-NIGER92 [e.g., *Gash et al.*, 1991]; SEBEX [*Wallace et al.*, 1991] in the Sahel of Africa; and in the Amazon region [e.g., *Shuttleworth*, 1985; *Wright et al.*, 1992; *Gash and Shuttleworth*, 1991; *Gash and Nobre*, 1997].

In our study, we have used the Regional Atmospheric Modeling System (RAMS) [*Pielke et al.*, 1992; *Nicholls et al.*, 1995] and observational data to investigate the significance of mesoscale fluxes as an important component of the heat fluxes over an observed heterogeneous distribution of surface characteristics, such as the one in the BOREAS region.

In section 2 we have discussed how the heterogeneity of surface physiography affects the heat fluxes in the region. Next, in section 3, linear analytical modeling results have been used to better characterize mesoscale effects and their scaling. Through these dynamical considerations we have defined the separation between mesoscale and turbulent processes.

In section 4, given the linear approach as a guidance, we have tested our ideas by forcing a coupled atmospheric-surface processes model with data describing the surface heterogeneity over BOREAS. We have set up numerical modeling experiments in order to assess the relative importance (as compared to turbulent processes) of the mesoscale circulations for one relevant case study. Finally, at the end of section 4 we have analyzed our modeling results for a mesoscale thermal signature, as we expected the effects of these mesoscale circulations to be identifiable as a time-integrated effect above the study region. Our conclusions are presented in section 5.

2. Description of the BOREAS Study Area

Most of the field campaigns mentioned in the previous section focused attention on the problem of scaling up surface fluxes from leaf-stand scale to GCM grid scale [*Sellers et al.*, 1995, Figure 2]. In FIFE, given the small study region (15 by 15 km) and the relatively homogeneous land cover, this was achieved with considerable success, although *Eastman et al.* [1997] and *Pielke et al.* [1997] proposed in their modeling studies that this kind of homogeneity in the surface fluxes can break down when cumulus convection is active or when the large-scale winds are weak.

Unlike FIFE, the BOREAS project covered a regional scale ($\sim 10^6$ km^2), over very heterogeneous terrain and land cover. Plates 1a and 1b were produced by using a land cover classification derived from the NOAA advanced very high resolution radiometer (AVHRR) data [*Steyaert et al.*, this issue]. Plate 1a covers most of the BOREAS domain; Plate 1b is a subset of Plate 1a, corresponding to the blue rectangle in Plate 1a.

We have included various types of ancillary information in these two figures to help identify items mentioned in this paper. The vegetation cover data set, originally in the Albers equal area projection, was remapped to geographic coordinates, for assimilation by our atmospheric model. The latitude-longitude reference lines and the provincial boundaries are indicated in black.

The RAMS grid number 1, corresponding to the domain of Plate 1a, comprised both the northern study area (NSA) and the southern study area (SSA), approximately covering the region from 52.09° to 56.60°N and 107.63° to 96.38°W (about 700 by 500 km), with a horizontal grid separation of 10 km. Grid 2 covered most of the SSA, from 53.42° to 54.29°N and 106.03° to 104.55°W (about 95 by 95 km), with a horizontal grid increment of 2.5 km. Grid 3 was designed to cover the region around Candle Lake, for comparison with aircraft observations, and comprised the region from 53.72° to 53.96°N and 105.5° to 105.1°W (about 24 by 26 km), with a grid separation of 625 m.

Within the study region (Plate 1a) there are numerous lakes (13% of the coverage by area), variable topography, several forest types, and large areas of burned vegetation in various stages of regeneration. A number of surface, airborne, and satellite measuring efforts (e.g., surface energy balance and biophysical characteristics) took place during BOREAS [*Sellers et al.*, 1995, Figures 2 and 4], providing good opportunities to evaluate if and when mesoscale circulations can become an important atmospheric feature in this region.

The boreal forest, as depicted in Plate 1a, is oriented diagonally from NW to SE, and some important gradients in biophysical parameters are therefore aligned with a SW-NE transect through the forest. From a larger-scale perspective (i.e., also encompassing BOREAS bordering regions), for instance, leaf area index (LAI) has a maximum over the forest, with minima farther south (agriculture, pasture) and farther north (tundra).

Over the southern BOREAS region, for the growing season, we identified at least five large groupings of land cover type which determine the surface fluxes: (1) forests, including wet

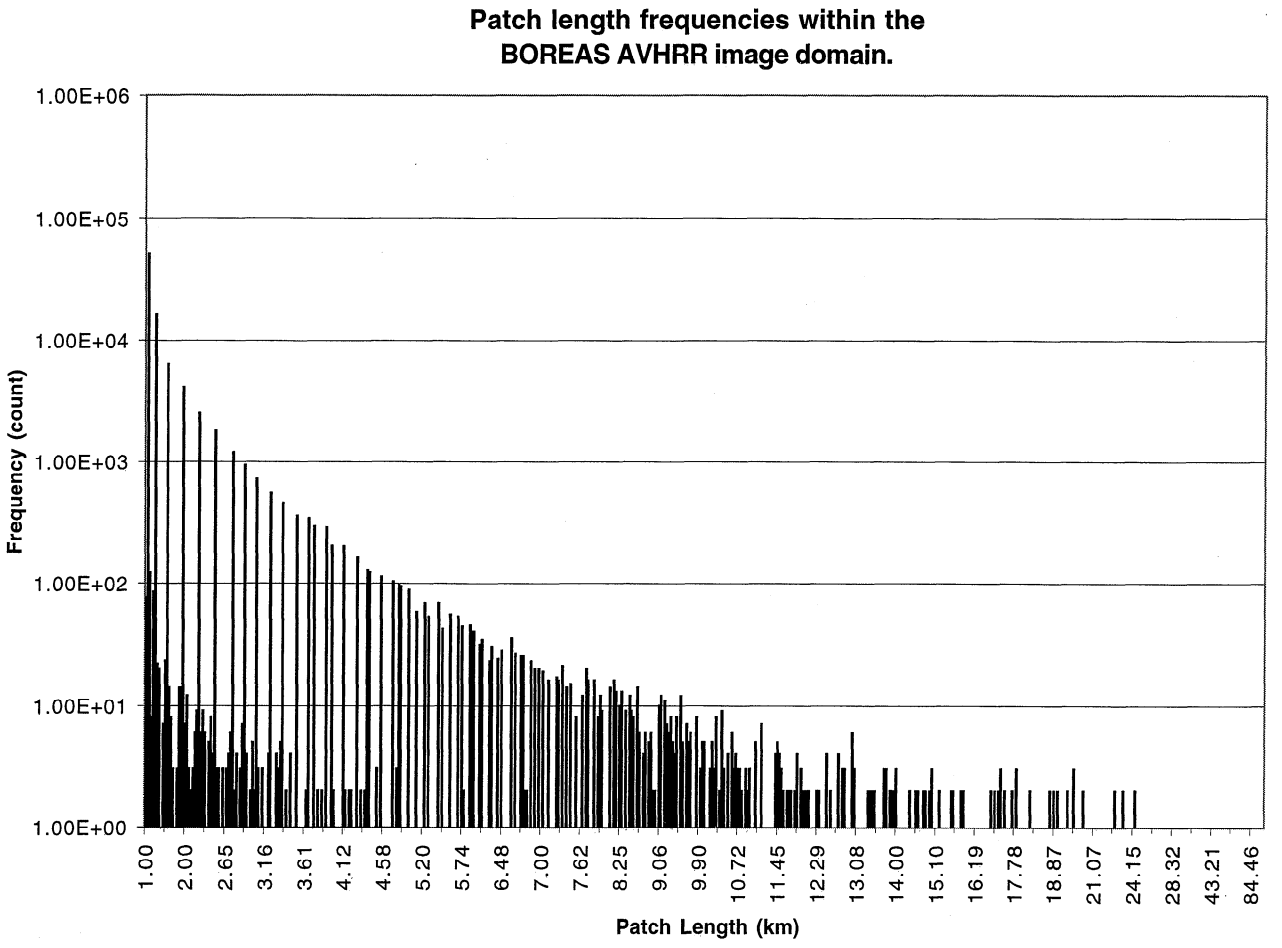

Figure 1. Patch length distribution for the BOREAS AVHRR classification over grid 1. Patch lengths (in kilometers) are shown on the x axis (data labeled in intervals of 100 elements); patch occurrence frequencies are shown on the y axis (logarithmic).

conifers (with albedos of about 10%); mixed forests (dominated by conifers); and deciduous trees (albedos of about 20%); all have high fractional vegetation coverage, high LAI, high roughness length, generally dry conditions (in terms of canopy-atmosphere exchanges, although the soils are predominantly wet); (2) recently burned regions, in some cases with dark albedos, comparable to water; (3) regeneration, with low LAI, low roughness length for recent stages of regeneration; higher LAI, high roughness length for older regeneration stages; (4) agriculture, with high albedo, low roughness length; (5) lakes, with low albedo, zero LAI, low roughness length.

Over the northern BOREAS region we can expect influences on surface fluxes to depend on the distribution of (1) forests: with low albedo, medium LAI, high roughness length, generally drier and colder conditions, as compared to the southern BOREAS region; (2) recent burns, some of which are 40–50 km in extent, with very low albedo; (3) regeneration, with variable vegetation composition and age, depending on the date of the last burn; (4) rock outcrops, with high albedo, low LAI, low roughness length, typically associated with burn scars; (5) lakes, with low albedo, zero LAI, low roughness length.

The landscape patchiness discussed above displays a non-random area frequency distribution, as shown by Figure 1, where patch area intervals are plotted versus area frequencies. While it is clear in this figure how the base AVHRR pixel size of 1 by 1 km dominates the distribution (also rendering the size distribution artificially discrete), hundreds of patches with areas of multiple hundred km^2 are present in the domain. The issue of the minimal patch size required for mesoscale atmospheric circulations to be forced by this patchiness will be discussed in section 3.

Biophysical characteristics are also quite heterogeneous within each class in Plates 1a and 1b, and gradients in LAI, fractional vegetation coverage, and vegetation height are quite pronounced. Furthermore, LAI and albedo display pronounced time variability within the growing season (see, for instance, the LAI product of *Chen and Cihlar* [1996]). The method of classification employed in building the BOREAS AVHRR land cover map attempted to address this problem by breaking classes into subclasses which included some degree of information about location and prevailing environmental conditions (e.g., regeneration north versus regeneration south, or high-density conifer versus low-density conifer versus upland dry conifer).

These elements of surface patchiness (which in our atmospheric model control the surface-atmosphere feedbacks), create horizontal gradients in surface and boundary layer (BL) heat fluxes, due to differential solar radiation absorption, evaporation, transpiration, and aerodynamic transfer, which may in turn generate mesoscale circulations.

An example of the resulting heterogeneity in fluxes mea-

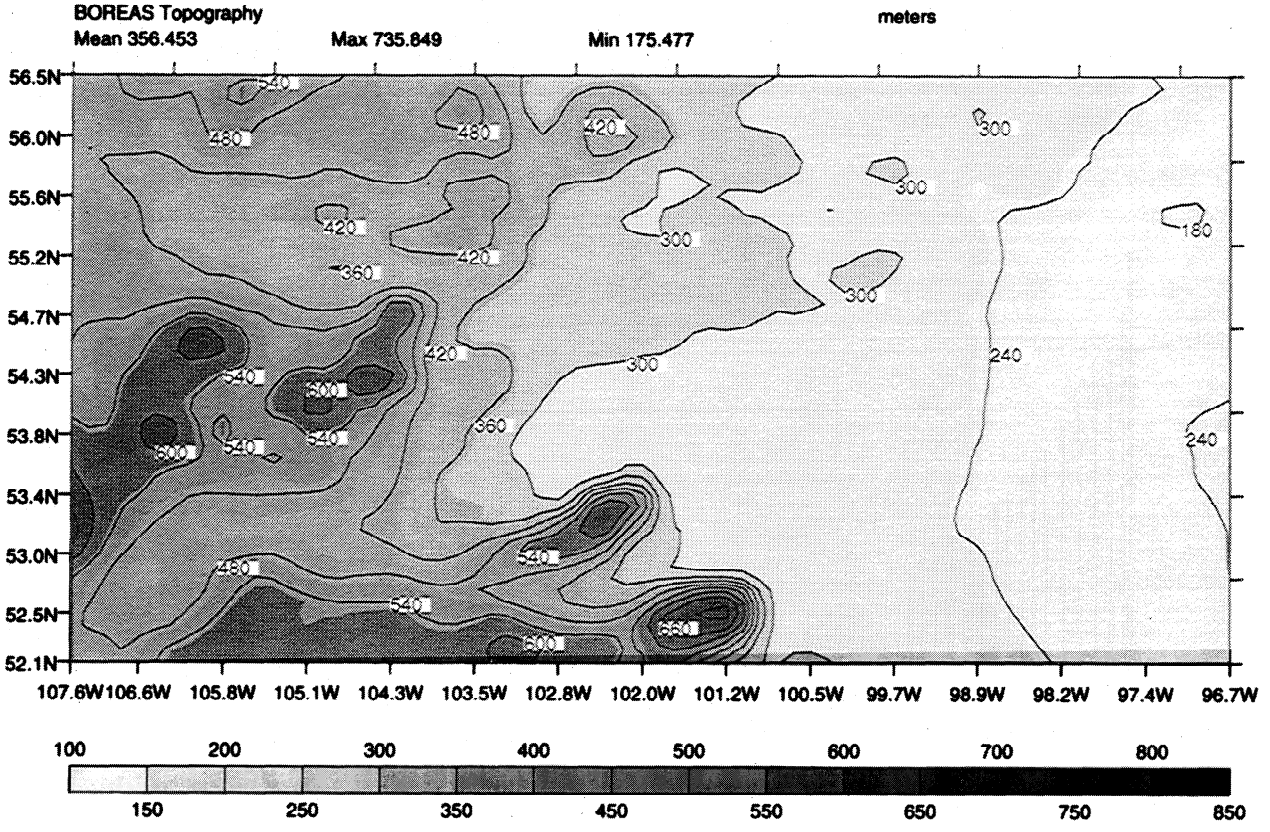

Figure 2. BOREAS regional 1 km topography. Reference lines are latitudes and longitudes in decimal degrees. Contour interval of 60 m.

sured during BOREAS is given by *Ogunjemiyo et al.* [this issue], who derived maps of average sensible and latent heat fluxes for the two study areas for each intensive field campaign (IFC) from the Twin Otter flights. A portion of the SSA, depicted as a red square on the right-hand side of Plate 1b, corresponds to the region over which the Twin Otter measurements were averaged to obtain mean IFC representation of diurnal fluxes of heat. Figure 6 in that paper [see *Ogunjemiyo et al.*, this issue] illustrates the existence of mean diurnal gradients, with maximum sensible heat flux near the dense conifer forest, measuring about 150 W m^{-2} over 10 km. These gradients are sustained both over the IFC timescale and over the whole growing season, and their value is sizable even though the surface heterogeneity (as characterized by the AVHRR product) over that area is not so pronounced as over other parts of the domain. It is interesting to notice that the spatial patterns obtained by averaging over all IFCs exhibit the strongest gradient for the all-IFC average along a SW-NE transect, colocated with the local topography gradient (Figure 2).

Another important element of surface heterogeneity is represented by the orographic features (Figure 2), which although not very pronounced are sufficient to induce horizontal gradients in the surface sensible heat flux, which in turn can generate mountain-valley flows. The BOREAS regional topography slopes from east to west and some hills are located within the SSA. Two other terrain features are present on the southern boundary of Figure 2; by comparison with Plate 1a it is interesting to observe how these local gradients in orography correspond to sharp changes in vegetation cover. Montreal Lake (SSA), Candle Lake (SSA, at the center of RAMS grid 3), and Lake Winnipeg (large lake in the southeastern region) are positioned near hilly terrain, as defined by the 1 km digital elevation model data set. The potential impact of orography over local circulations will be explored in section 4.2.2 by analyzing the wind fields produced by our numerical model.

3. Role of Turbulent and Mesoscale Fluxes in the BOREAS Region: Interpretation From Linear Theory of Mesoscale Circulations

Many authors have given definitions of atmospheric scales, some based on spatial and time categories [e.g., *Orlanski*, 1975], others using dynamical approaches [e.g., *Ooyama*, 1980]. Here we make use of dynamical definitions, after a short review of past theoretical work.

Referring back to linear theory, *Dalu et al.* [1996] have given some guidance as to the expected impacts of mesoscale circulations under weak synoptic wind conditions. Vertical profiles through the low to middle troposphere [e.g., *Dalu et al.*, 1996, Figures $3a_2$, b_2, c_2] depict the impact of the heating caused by a solenoidal circulation generated by differential surface diabatic heating (in this case, an idealized sea-land contrast) on the atmosphere. This impact translates into heating at lower levels, within the depth of the convective boundary layer (CBL), and a cooling above it, up to about twice the depth of the CBL. The intensity of the heating depends on basic-state wind magnitude, with lower differential heat fluxes corresponding to a high wind situation, in which the horizontal surface heating gradient, i.e., the mesoscale available potential

energy, is reduced by the prevailing flow [also see *Dalu et al.*, 1996, Figure 5d]. In the presence of sustained synoptic flow, differential surface roughness effects become predominant and the mesoscale perturbation is in the form of propagating waves that penetrate deep into the free atmosphere, causing a net downward flux of momentum, which is dissipated within the CBL by turbulence. Above the CBL, mixing with the environment of the air particles displaced by the waves results in a net negative mesoscale heat flux. These findings are also supported by the work of *Wang et al.* [1997], using a nonlinear numerical model.

The mesoscale heat fluxes are characterized by different timescales than the turbulent heat fluxes, tending to reach peak magnitude later in the diurnal cycle. The time phase lag is about 2 hours, as results from (1):

$$T = \frac{1}{\sqrt{f^2 + \lambda^2}} \tag{1}$$

where f is the local Coriolis parameter (here 10^{-4} s^{-1}) and λ corresponds to a linearized friction term (here a value of $\lambda \leq 10^{-4}$ s^{-1} is used as given by *Haurwitz* [1947]).

In terms of cell dimensions these studies suggested that the maximum horizontal extension of the circulation cells is of the order of the local Rossby radius (defined as (2)), while the vertical extent is of the order of the depth of the CBL. They also pointed out that these scales define lower and upper limits for the existence of these circulations in terms of the spatial scale of the forcing (i.e., the size of the landscape inhomogeneities).

From linear theory applied to the BOREAS region, the local Rossby radius (R_0) is of the order of 100 km or smaller, calculated from

$$R_0 = \frac{N \cdot z_i}{\sqrt{f^2 + \lambda^2}} \tag{2}$$

where N is the Brunt-Väisälä frequency (depending on the stability, a value of $N = 5 \times 10^{-3}$ s^{-1} will give $R_0 \simeq 70$ km, a value of $N = 1 \times 10^{-2}$ s^{-1}, close to climatology, will give $R_0 \simeq 140$ km); z_i is the CBL depth (here assumed 2000 m).

Theoretical results from *Dalu et al.* [1996] showed that the strongest mesoscale flows occur when the horizontal wavelength of the inhomogeneities are of the order of two local Rossby radiuses and become negligible when this wavelength is of the order of twice the depth of the CBL.

Turbulent processes are defined therefore, in the context of our specific BOREAS case study, as having timescales much smaller than the diurnal timescale and spatial scales under 4 km. Mesoscale processes are defined as having timescales comparable to the diurnal timescale and spatial scales between 4 km and 280 km, corresponding approximately to Orlanski's meso-γ and meso-β categories. Synoptic scale refers here to timescales of multiple days and spatial scales above 280 km.

From the point of view of the surface forcing scales acting on atmospheric circulations, it is therefore to be expected from the previous analysis that patches contained within twice the local Rossby radius (but larger than twice the CBL) will be influenced by mesoscale circulations. It is easily seen from the BOREAS vegetation coverage map (Plate 1a) that most of the central and northeastern part of the domain will have overlapping influence regions due to the spatial distribution of the landscape heterogeneities, including lakes.

The relevance of this type of idealized study for BOREAS lies in the fact that organized land cover patchiness has been shown observationally to induce horizontal diabatic heating gradients that are as intense as the ones present in a sea breeze case (e.g., *Segal et al.* [1989], for irrigated regions in Colorado). The measurements of *Ogunjemiyo et al.* [this issue] as well as observations discussed later in this paper document the existence of such gradients.

4. Role of Turbulent and Mesoscale Fluxes in the BOREAS Region: Interpretation from Mesoscale Numerical Modeling

The analysis stemming from atmospheric dynamics in the previous section suggested scaling rules that we applied directly in our modeling strategy. Thus, for this region, we recognized that patch scales under about 4 km would not be capable of forcing mesoscale circulations, and their fractional contributions to heat fluxes could be summed linearly. Good examples of this unresolved patchiness (meaning that the atmospheric model is not explicitly capable of correctly nor completely representing the influence of these scales) is illustrated by some of the smaller lakes, with areal extents as small as 1 by 1 km, and the fen class distribution, which is clearly limited to scales under a few kilometers and is absent from the AVHRR 1 km land cover product (Plates 1a and 1b), because of inherent technical limitations. At scales between about 4 km and 280 km, however, we should consider nonlinear interactions between patches, which dictated our lowest resolution needs for the explicit representation of landscape heterogeneity and its feedback to the atmosphere.

4.1. RAMS Configuration

Given this theoretical guidance, numerical simulations were performed with RAMS using a two-way, interacting nested grid configuration which allowed us to focus on the study areas with increasing resolution. The horizontal grids were described in section 2. The vertical grid increment was initiated and calculated at 30 m above ground level (so the first atmospheric level corresponded as nearly as possible to that of most aircraft measurements, although most of the near-surface analysis presented in this paper is at 60 m, because of the vertical grid stagger) and was then telescoped upward through 28 levels, with the model top at 12,000 m on average, depending on the surface terrain.

The soil-vegetation-atmosphere transfer scheme (SVATS) used in RAMS is the LEAF-2 submodel [*Lee*, 1992; R. L. Walko et al., manuscript in preparation, 1997], which is a one-level canopy model capable of representing the surface energy balance as mediated by surface aerodynamics [*Louis et al.*, 1981], parameterized canopy conductance [*Jarvis*, 1976], and multilevel dynamic soil processes [*Tremback and Kessler*, 1985]. Within each LEAF-2 grid cell, a number of surface cover patches coexist, with a minimum number of two (one water body and one vegetation type) and a maximum number limited by computer resources. Quantities which are averaged linearly by patch fractional area are the actual surface fluxes and not the patch biophysical characteristics, in agreement with the discussion of *Sun and Mahrt* [1995] and *Mahrt et al.* [this issue] on the computation of fractional contributions to surface fluxes.

A secondary objective of running RAMS over a few days during IFC-2 was a basic validation of LEAF 2, through comparison with IFC data sets. Our primary focus, however, was to

contrast the relative contributions of turbulent (parameterized) and mesoscale (resolved) heat fluxes. This determination has a very important impact for the scaling-up process and could quantify the effect of local circulations on point measurements (e.g., tower fluxes). A good example is given by nocturnal CO_2 flux (coming from respiration), which could be underestimated if a cold drainage flow transports the CO_2-rich air in the surface layer away from the measuring site and concentrates it in a terrain depression (e.g., Candle Lake; see also *Sun et al.* [1997]), to later vent it out of the nocturnal layer through vertical motion at the lake center. The technique used to separate mesoscale and turbulent quantities for this part of our study was based on the one described by *Mahrt et al.* [1994b]. In the model this translated into calculating domain averages by layer and deviations from this average at each grid point. Correlations of these resolved perturbations were then used to compute resolved fluxes.

4.1.1. RAMS boundary conditions. The surface vegetation characteristics were defined by using the AVHRR vegetation classification (Plate 1a) which has nominal resolution at 1 km and actual useful resolution at 2–3 km. Grid 3 was designed therefore to be able to resolve the finest scales defined by this product; grids 1 and 2 were initialized, for separate model runs, by the use of a predominant pixel or by a mosaic [*Avissar and Pielke*, 1989] technique. Other surface boundary conditions included 1 km digital elevation maps (DEMs), surface water bodies (defined by the AVHRR product), and soil-type distribution, which were interpolated to each grid.

4.1.2. RAMS initialization. The initial meteorological conditions and the hourly grid 1 boundary conditions (outer five points) were derived from the United States ETA model analysis [*Black*, 1994] at 0000 and 1200 UTC, using the *Davies* [1983] technique. Surface water temperature was defined by using aircraft measurements [*Sun et al.*, this issue]. Extensive use of the BORIS (BOREAS Information Service) data sets allowed us to refine the model initialization locally with all available information from observations, especially in the case of soil data (e.g., profiles of initial soil water content and soil temperature, which were locally distributed according to vegetation type). After doing this, the model was allowed to run for more than a full diurnal cycle (two nights and one day) before using its output for analysis. This was to permit the soil heat and moisture component of the model to adjust to the atmospheric forcing.

4.2. July 21 "Golden Day"

This day was selected because of its relevance to the rest of the BOREAS community; it presented very clear skies and was ideal for radiative transfer work. The synoptic scale winds in this case study were not weak, reaching 10 m s^{-1} at the surface during the day and over 11 m s^{-1} during the night; so this was certainly not an ideal case for mesoscale circulations [*Dalu et al.*, 1996; *Wang et al.*, 1997]. The July 21, 1994, case was simulated by initializing the model on July 20 at 0000 UTC (July 19, 1800 LT) and running RAMS for 60 hours, as mentioned above. The temperature of the Candle Lake water (and of every other lake in the domain) for July 20–22, 1994, was set at 283 K. Soil temperature and moisture profiles were initialized by using information from the automated meteorological stations (AMS) and the Atmospheric Environmental Services (AES) network on July 20.

4.2.1. Validation and comparison with aircraft observational evidence. Flux aircraft measurements at various heights (for instance, 30 m for the NOAA LongEZ, 100 m and more for the NCAR Electra) offered additional evidence of the very heterogeneous horizontal distribution of surface fluxes of heat, moisture, momentum, and CO_2, calculated by eddy correlation techniques. Transects over the Candle Lake region in the SSA comprised regions predominantly covered by deciduous trees (aspen) in the west, transitioning into a mixed forest cover and, proceeding eastward, into a wet conifer region (black spruce, jack pine, fens, bogs). Special model slices through grids 2 and 3 were generated, corresponding to aircraft transects. Figure 3 (data here reproduced with permission of Crawford and Baldocchi) shows temporally averaged sensible and latent turbulent fluxes, measured by the NOAA LongEZ aircraft over 13 legs between 15.32 and 23.20 UTC on July 21, 1994 (transect indicated in Plate 1b). In particular, the LongEZ measurements of sensible heat over Candle Lake for July 21, 1994, showed a sharp reduction from about 275 W m^{-2} to almost -30 W m^{-2} when moving from the forested regions around the lake to a position directly over the lake. The magnitude of the fluxes and their horizontal gradients over this transect were found to be very similar to others measured during July 1994 by the LongEZ aircraft and not an example of a single occurrence.

Figure 3 also shows the turbulent fluxes modeled by the LEAF-2 RAMS submodel, temporally averaged through the same period. The model was capable of capturing the spatial pattern of the fluxes quite accurately. The magnitudes of the fluxes were also in reasonable agreement, even without any special tuning of the model parameters that control canopy conductance. For the correct interpretation of the comparison between the two data sets, it is important to remember that the model fluxes are representative of a set of volume averages over grid cells corresponding to the aircraft transect, while the aircraft fluxes are transect and time averages.

Referring to Plate 1b, the SW land cover has contributions from the deciduous forest and disturbance classes (higher albedo, lower LAI), while the NE displays lower albedo (conifers) and some patches of drier soils (for the uphill dry conifer). The modeled gradient was not as finely resolved as the measured one, but it is clear from the plot that the horizontally integrated heat input from the surface east of the lake was higher than that from west of the lake. The modeled sensible heat flux maximum, of 275 W m^{-2}, was (at point locations) about 75–100 W m^{-2} higher than observations, especially on the west side of the lake, while the latent heat flux was about 30 W m^{-2} lower on average than the observed one.

Previous sensitivity tests suggested that the main controlling parameter for the surface fluxes calculated in the present version of LEAF 2 is the leaf area index. LAI was here indirectly specified (with a look-up table (LUT) approach) by the land cover classification and not linked to remote sensing, so the modeled spatial gradients in vegetation parameters are only representative at scales larger than actually occur along this transect (i.e., the aircraft, of course, measured fluxes from all patch sizes in the flight cross sections, while the model used patch data that were limited to 2–3 km of effective resolution). The horizontally homogeneous sensible heat flux plateaus over the mixed forest class on the west portion of the graph are also indicative of how the LUT approach is not capable of representing intraclass heterogeneity of biophysical parameters.

The important point for the modeling results described in

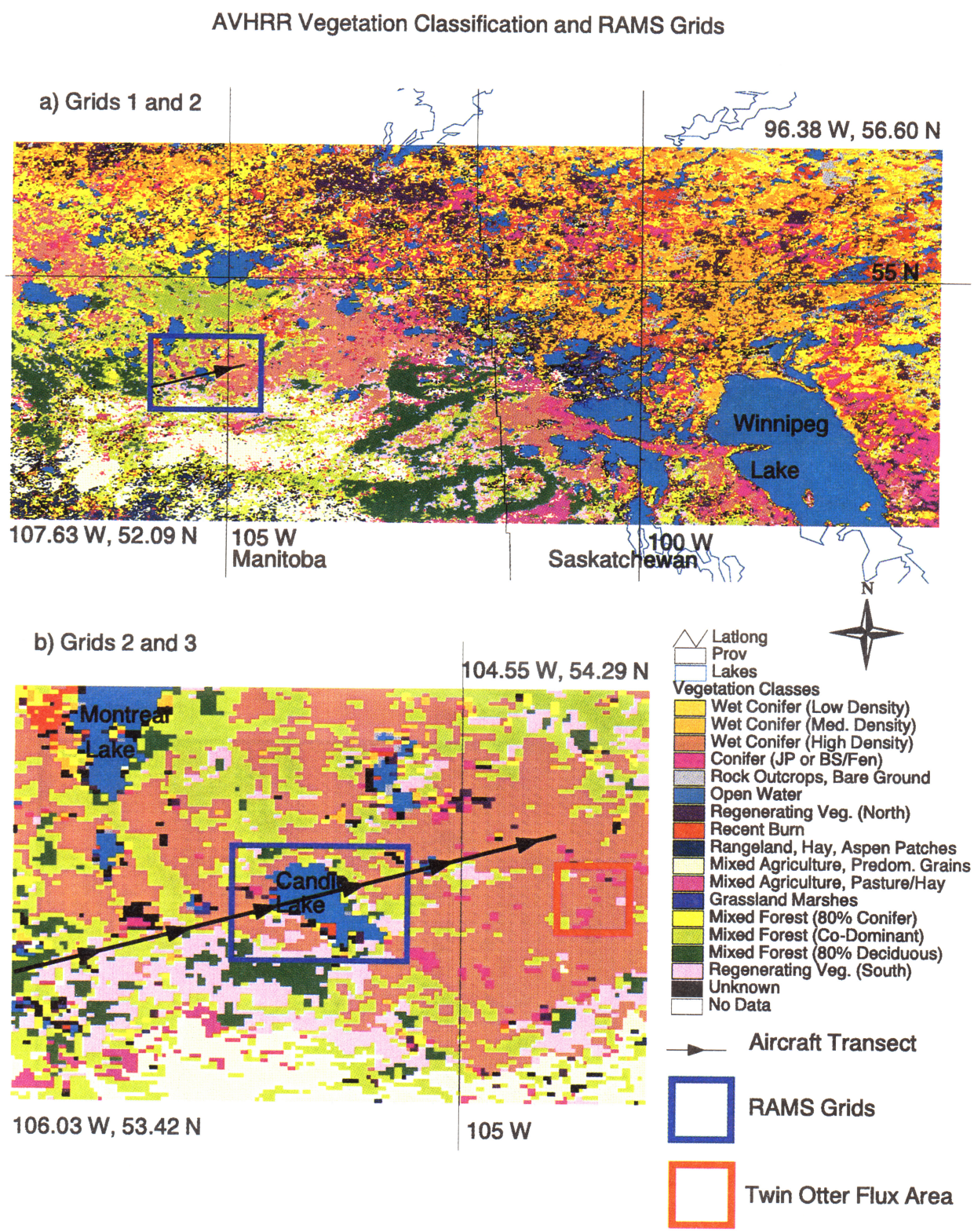

Plate 1. (a) AVHRR 1 km BOREAS regional land cover classification. Dark lines and letters indicate latitudes and longitudes with an interval of 5°. The map corresponds to RAMS grid 1 (52.09° to 56.60°N and 107.63° to 96.38°W); (b) AVHRR 1 km BOREAS regional land cover classification for RAMS grid number 2. Dark lines indicate latitudes and longitudes in degrees with an interval of 0.5°. The map limits are 53.42° to 54.29°N and 106.03° to 104.55°W. The red rectangle corresponds to the Twin Otter integrated flux region. Other symbols are explained in the legend.

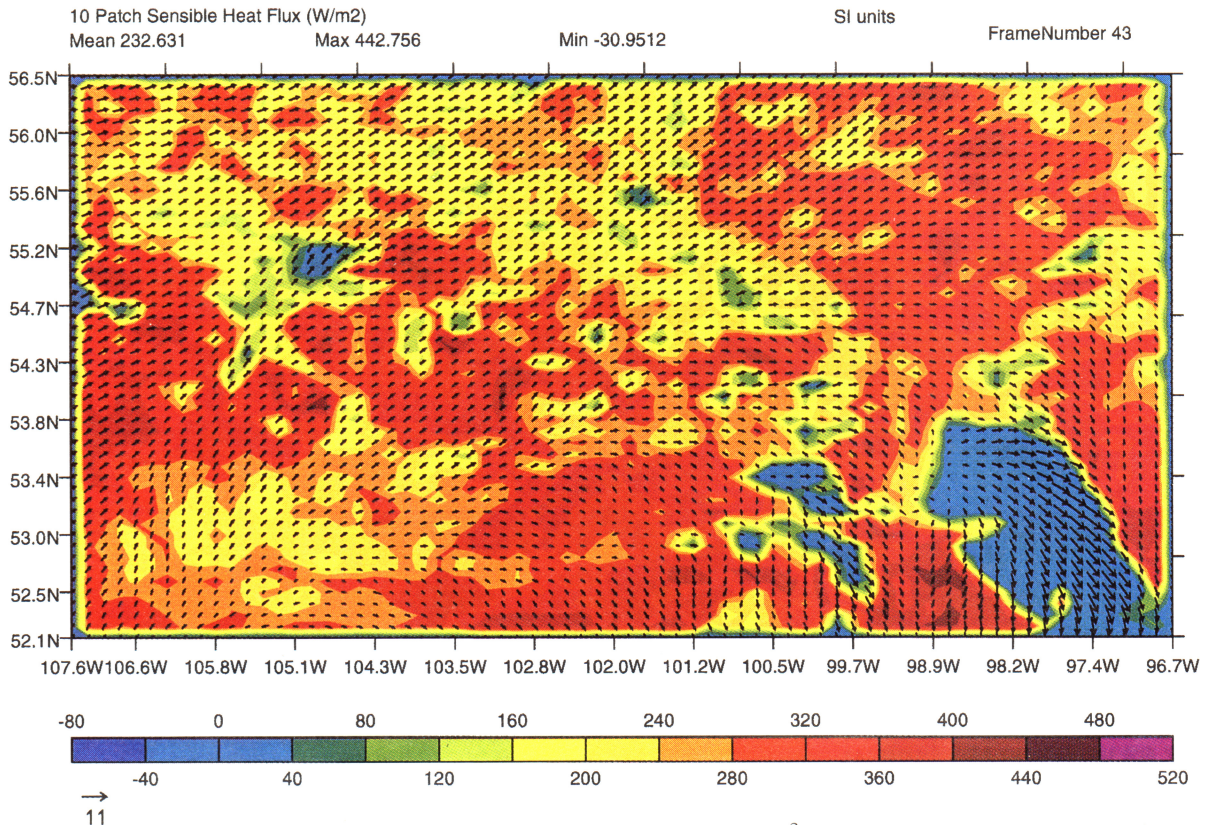

Plate 2. Coarse-grid run: the grid 1 surface sensible heat fluxes (W m^{-2}) at 1900 UTC, July 21, 1994, and the near-surface (60 m) wind vectors. The color field and color bar represent the turbulent sensible heat flux. Reference lines are in decimal degrees.

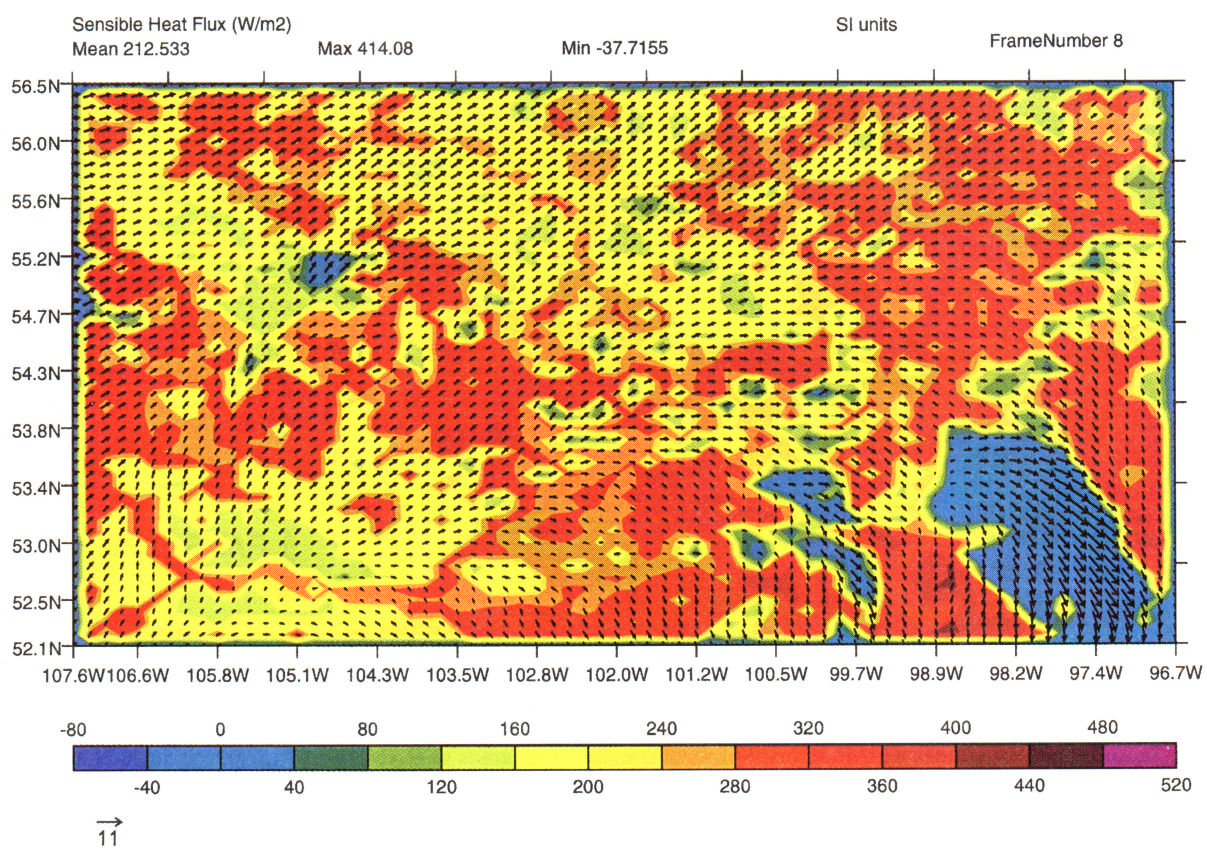

Plate 3. Fine-grid run: the grid 1 surface sensible heat fluxes (W m^{-2}) at 1900 UTC, July 21, 1994, and the near-surface (60 m) wind vectors. The color field and color bar represent the turbulent sensible heat flux. Reference lines are in decimal degrees.

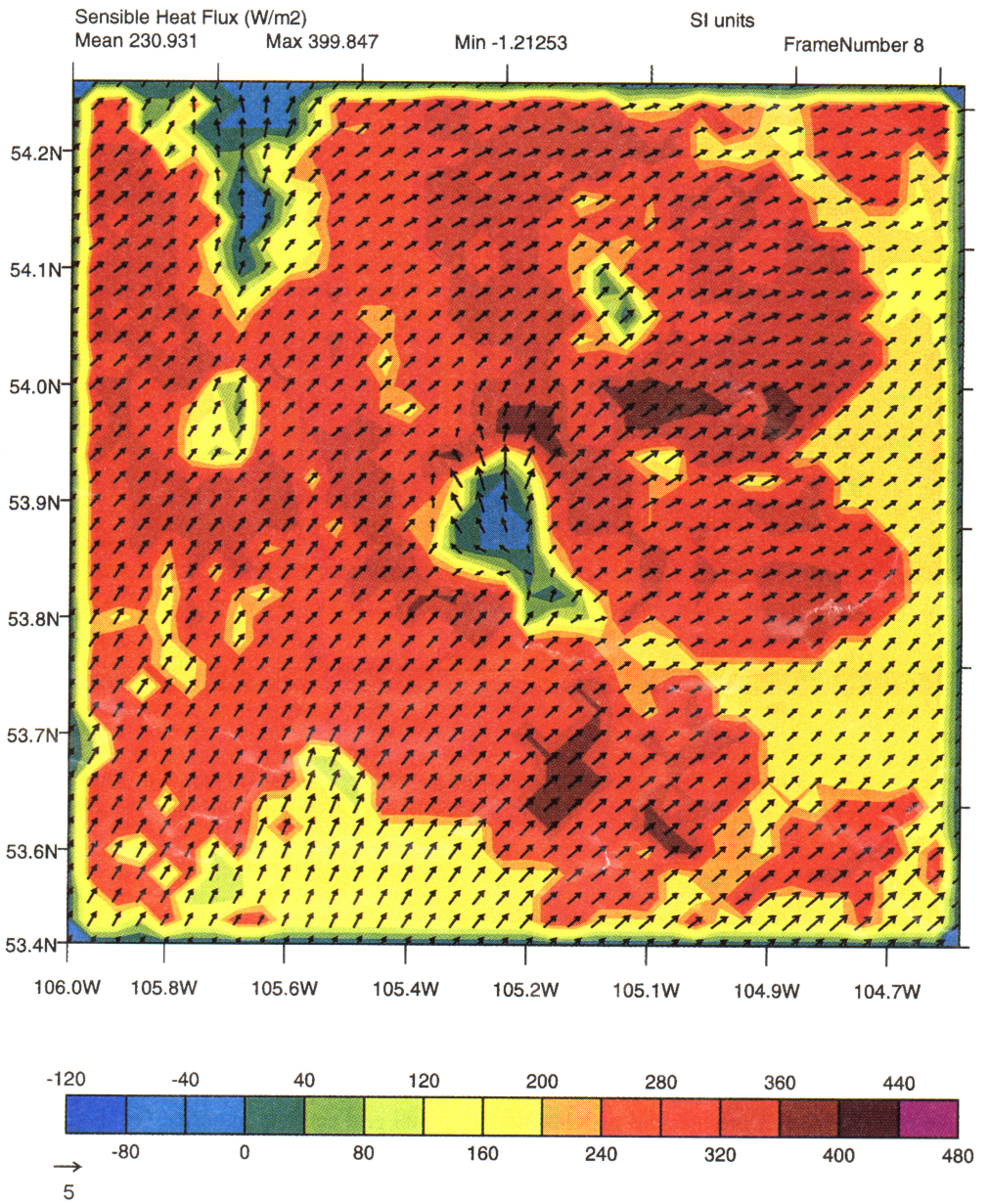

Plate 4. Fine-grid run: the grid 2 surface sensible heat fluxes (W m^{-2}) at 1900 UTC, July 21, 1994, and the near-surface (60 m) wind vectors. The color field and color bar represent the turbulent sensible heat flux. Reference lines are in decimal degrees.

the following sections was that the gradient between Candle Lake and its surrounding measured (at its peak time) over 300 W m^{-2} over about 20 km and according to linear theory was sufficient to force a mesoscale circulation under the proper synoptic conditions. For a maximum effect to occur, linear theory [*Dalu et al.*, 1996] suggests that the two coastal breeze cells should constructively interact at the lake center to form a maximum subsidence and surface divergence pattern, lagging by about 2 hours the time of maximum diurnal heating.

Occurrences of a lake breeze over Candle Lake were successfully simulated with our atmospheric model for some calm wind days in June (IFC-1) and July (IFC-2) 1994, and their divergence/convergence patterns agreed well with the analysis of *Sun et al.* [this issue], which was conducted for Candle Lake during similarly calm days. The contrast could also be seen in the temperature gradient over the same transect for the summer season [*Sun et al.*, Figures 2a and 2b, this issue]. On July 21, 1994, the date of our model simulation in this paper, a diurnal evolution of the horizontal wind divergence over the center of Candle Lake, derived from data of the LongEZ aircraft (Figure 4, data reproduced with permission of J. Sun), appeared as a clear lake breeze signature. The timing of the divergence pattern reflects both the 2 hour lag mentioned in section 3 and the fact that the breeze cell was displaced to the NW, as will be shown in section 4.2.4. The mass divergence measured about 0.0002 s^{-1} during the heating period, between 1300 and 1700 LT (1900 and 2300 UTC), while a convergence (negative divergence, with peak of -0.0005 s^{-1}) was still present between 0900 and 1200 LT at the end of the nocturnal cooling period.

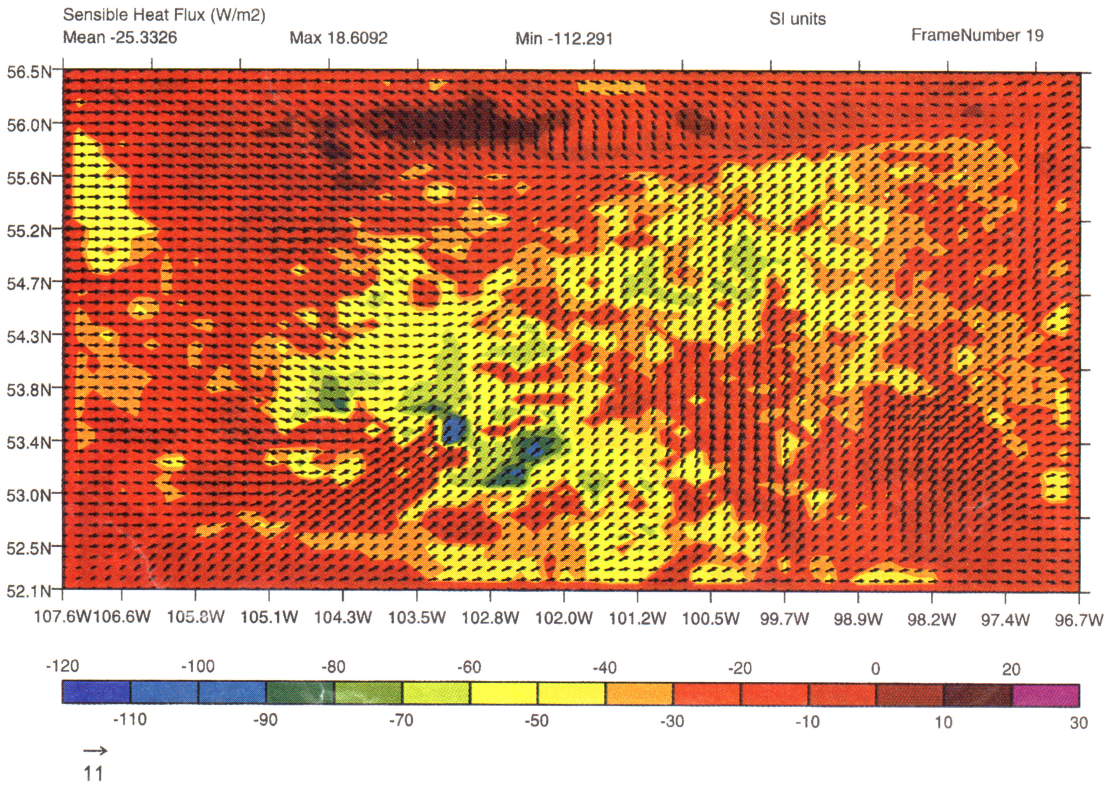

Plate 5. Fine-grid run: the grid 1 surface sensible heat fluxes (W m^{-2}) at 0600 UTC, July 22, 1994, and the near-surface (60 m) wind vectors. The color field and color bar represent the turbulent sensible heat flux. Reference lines are in decimal degrees.

4.2.2. Fluxes in grid 1 (Δx = 10 km). The grid 1 integration was carried out in two fashions by specifying the land cover over each grid cell at two different resolutions: (1) coarse-grid run, with grid separations as low as 10 km, in which the contributions from classes in the AVHRR product were included by statistics and the mesoscale was not fully resolved; (2) fine-grid run, with grid separations as low as 625 m, in which the resolution of the AVHRR product was matched at each grid point within grid 3 (and the mesoscale was fully resolved within this finest mesh); this is the same run that was discussed in section 4.2.

For the coarse-grid case we used a 10-patch representation of surface characteristics, while for the fine-grid case, we used a 2-patch (predominant pixel) representation. The choice of 10 patches was based on the number of existing vegetation classes (18) in the AVHRR product and on the high correlation between soil type and land cover class, so we could ensure a good statistical representation of the local heterogeneity with 10 km horizontal grid spacing. The 2-patch approach in the fine-grid run is the minimal LEAF-2 configuration and consists of using one vegetation type and one water patch per grid cell.

In both cases, RAMS was initialized at 0000 UTC on July 20, 1994, using the ETA analysis, and then nudged over grid 1 exclusively. For the fine-grid run, after one complete diurnal cycle grids 2 and 3 were spawned and surface-atmosphere fluxes at scales as small as 2.5 km (corresponding to the 625 m grid spacing, since the resolution is defined as 4 × Δx; see discussion by *Pielke* [1984, page 327]) were explicitly calculated over these finer meshes for a second, complete diurnal cycle. In the coarse-grid case we were relying on a mosaic approach [*Avissar and Pielke*, 1989], and the nested grids were never spawned, thus truncating our effective resolution to 40 km, which limited our ability to represent surface heat flux gradients and associated mesoscale atmospheric circulations.

In terms of a local enhancement of turbulent effects, for example, a lake with dimensions of less than 10 by 10 km only contributed to the surface parameterized (turbulent) sensible heat fluxes as a grid cell fractional component, thus lowering the total grid cell flux intensity. On the other hand, a lake of similar size, within the fine mesh (grid 3), was capable of cooling the atmosphere above it directly and, through resolved advection of cooler air, of ultimately enhancing the turbulent sensible heat fluxes from the land surrounding it.

The grid 1 sensible heat fluxes at 1900 UTC (1300 LT) on July 21 (Plate 2) showed some general differences, in that the coarse-grid run produced slightly higher domain average surface sensible heat fluxes (differences of about 30 W m^{-2}) than the fine-grid run. The predominant pixel technique in the fine-grid run favored forests (which are more abundant and have larger patch scale) over disturbance regions, which are not very spatially organized and have larger albedo, smaller LAI, higher bare soil fraction, and lower roughness length. Locally, however, for example, in the Candle Lake (105.3°W, 53.8°N) and Montreal Lake regions, the coarse-grid run produced patches of flux minima, whereas the fine-grid run produced sharper flux gradients between lake and forest. Again, this is indicative of the different impact of a "fully resolved" versus a "mosaic" treatment of local surface flux gradients and the associated near-surface wind circulations.

It is also possible to confirm that the orography has a local control on the wind patterns by contrasting the day-night surface wind maps over Plates 3–6 with the topography map in

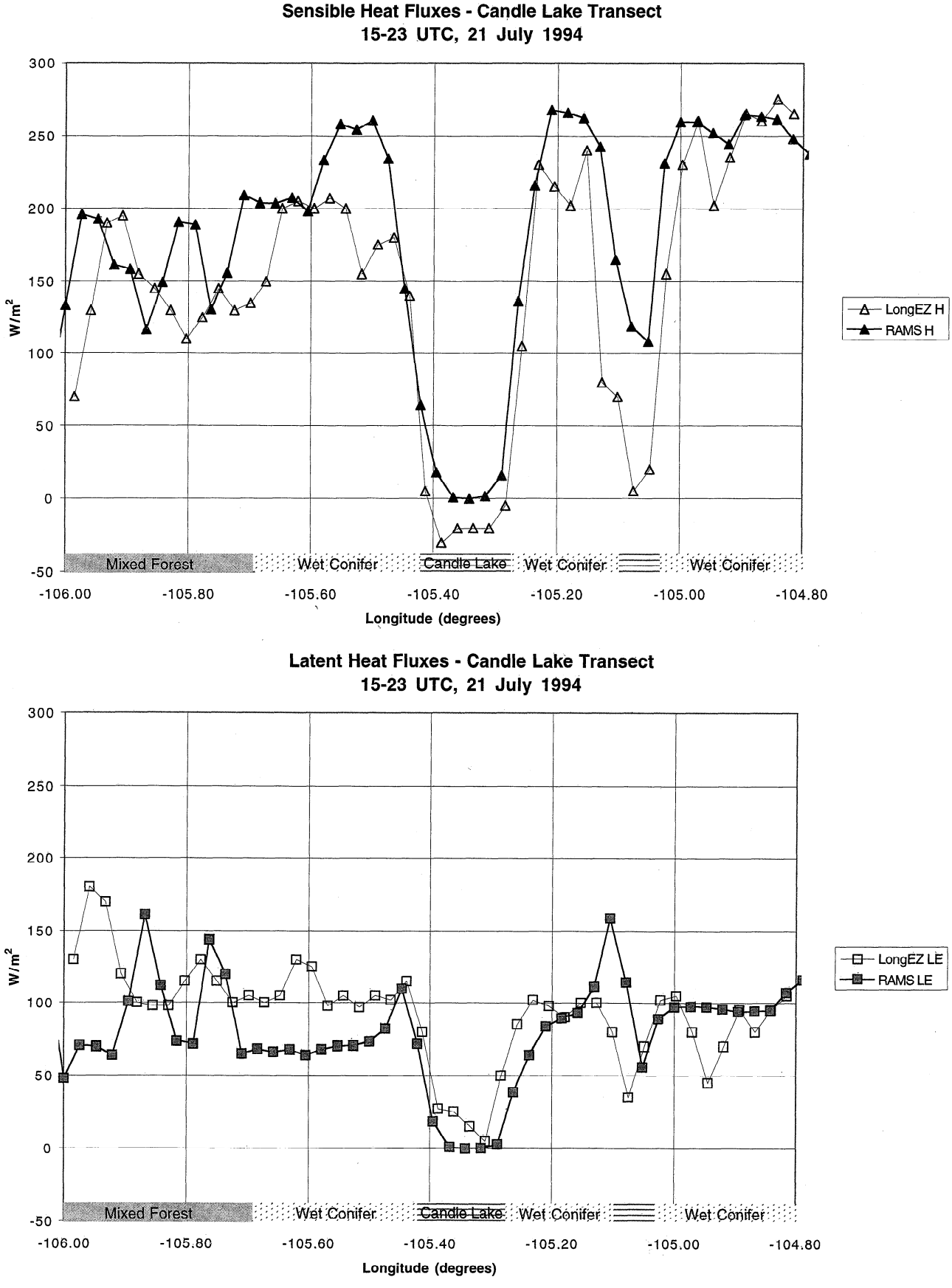

Figure 3. RAMS and NOAA LongEZ (provided by Crawford and Baldocchi) transect surface turbulent fluxes (W m^{-2}) for the SSA, averaged between 1500 and 2300 UTC, July 21, 1994. Sensible heat fluxes are labeled H, latent heat fluxes are labeled LE. Predominant surface vegetation types, as interpreted from aircraft data, are indicated along the transect.

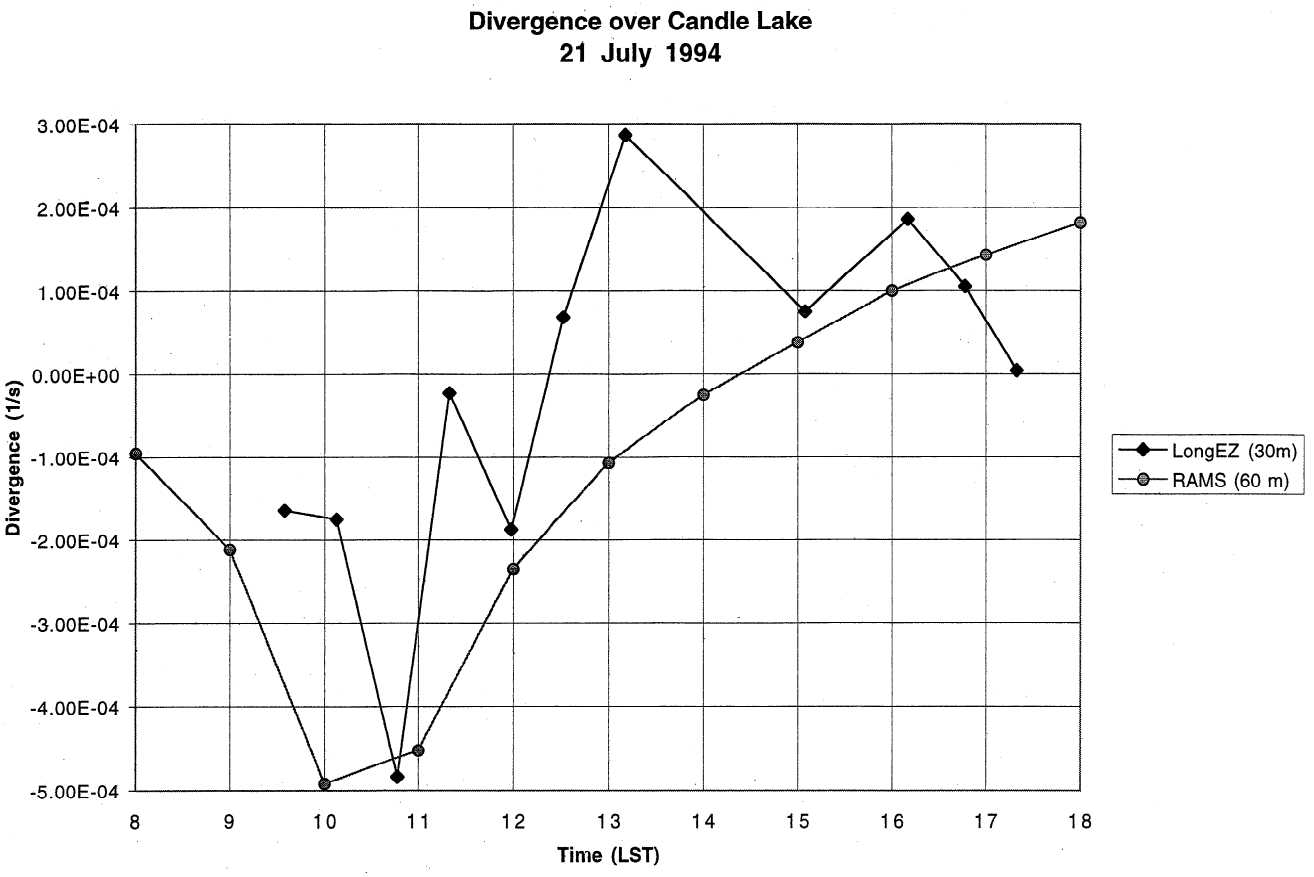

Figure 4. Wind divergence (1/s) over the center of Candle Lake on July 21, 1994, between 0800 and 1800 LST, as calculated from wind measurements of the NOAA LongEZ at 30 m (data provided by J. Sun) and RAMS 60 m divergence (1/s) at corresponding times and locations within grid 3.

Figure 2. In these four wind maps we have used a color representation of the surface parameterized sensible heat flux, which helps point to the presence of lakes (minima, corresponding to flux into the water), and wind arrows to represent the horizontal wind at 60 m.

During the day, for the fine-grid run in the grid 2 region, a prevailing southwesterly flow turned northward in the direction of the local slope gradient, with a clear convergence signal on the northern boundary of Candle Lake (center of grid 2) and a divergence signal on the E and NE parts of the lake. The turning and acceleration of the wind to the N of Candle Lake was due to a combined effect of the lake breeze and of the uphill flow. On the NE part of the grid 2 domain the flow turned eastward, again in the direction of the slope.

During the night, over both grids (Plates 5, 6), the flow turned locally to SE, showing a tendency to join the drainage flow to the SE (53.5 S, 103.5 W). The local divergence and turning were stronger in the SE portion of the grid 2 domain (Plate 6), aligned with the local slope. At the center of grid 2, over Candle Lake, there was local acceleration of the wind, due to decoupling caused by the formation of an intense nocturnal layer at the lake center (not shown).

Some larger features on the SW region of grid 1 (Plate 5) were also capable of generating local circulations, even at 40 km resolution. The two terrain features on the southern boundary of grid 1 influenced the local flow, with uphill motion during the day and drainage during the night. The southwesterly flow to their west turned westerly to northwesterly locally, in the direction of the slopes. The divergence/convergence pattern over Lake Winnipeg (bottom right of Fig. 9) was also a very clear example of a local differential heating effect influencing atmospheric motions.

The coarse-grid run did not display the same local circulation characteristics around the grids 2 and 3 region, although retaining some of the flow sensitivity to larger scale features.

4.2.3. Fluxes in grid 2 (Δx = 2500 m). Sensible and latent heat fluxes were calculated both at the subgrid (parameterized turbulence) and at the resolved scales. The fluxes were later analyzed near the level at which they typically displayed maximum magnitude.

4.2.3.1. Parameterized turbulent fluxes: Following the discussion in the previous section, turbulent surface sensible heat fluxes were quite pronounced over the grid 2 region. This could be explained by the large LAI of dense conifer but also to horizontal advection of cooler air due to mesoscale circulations caused by differential heating between slope and valley (e.g., the local depression where Candle Lake is located), as discussed previously. The lowest sensible heat fluxes were found to correspond to the positions of Candle Lake (center) and Montreal Lake (NW). As a confirmation of the characteristics of the air advected from Candle Lake, Figure 5 shows a potential temperature transect through Candle Lake roughly corresponding to the NOAA LongEZ transect. In this figure it is possible to see how the influence of Candle Lake (lakes are indicated by contours near the surface) on the potential temperature profile, in conjunction with predominant southwest-

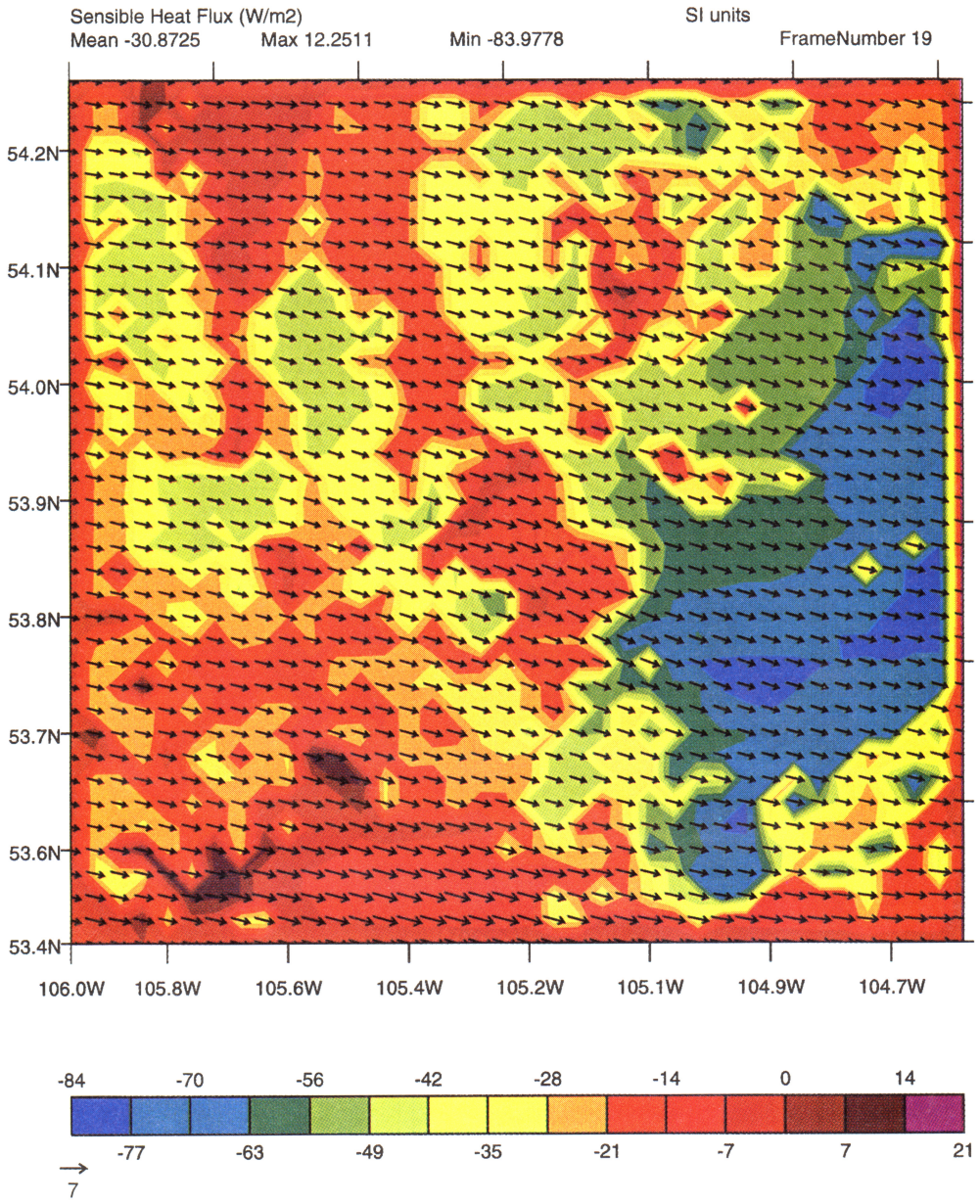

Plate 6. Fine-grid run: the grid 2 surface sensible heat fluxes (W m^{-2}) at 0600 UTC, July 22, 1994, and the near-surface (60 m) wind vectors. The color field and color bar represent the turbulent sensible heat flux. Reference lines are in decimal degrees.

erly flow, induced the formation of an internal boundary layer on the east bank of the lake, with a surface layer temperature change of 1 K over about 20 km between the two shores of the lake.

Turbulent fluxes over the grid 2 domain appeared to be highest around 1900 UTC, with maxima of almost 400 W m^{-2} and presented large horizontal gradients associated with the vegetation cover type (Plate 4). The wet conifer class (mainly black spruce, *Picea mariana*) generated the more intense sensible heat fluxes, as was also shown by the aircraft data. The lowest turbulent sensible heat fluxes were found to be concentrated in the southern portion of the grid 2 domain, where the forest transitions to agriculture. The latent heat fluxes (Figure 6) were, on the other hand, much more homogeneous and had localized maxima of almost 270 W m^{-2}, mainly associated with the mixed forest cover class.

4.2.3.2. Mesoscale (resolved) fluxes: Mesoscale fluxes over grid 2 (with contributions from grid 3, through the two-way nesting), calculated from the correlations of domain 2 average (a size comparable to the local Rossby radius) residuals of temperature and vertical velocity (for sensible heat), displayed maxima at higher levels (as compared to turbulent fluxes, which typically decay with height), in the upper portion of the BL. Their depth was typically confined to a layer of about 2000 m. The first substantial mesoscale sensible heat flux (small patches with maxima up to 270 W m^{-2}) was produced by the model at 2200 UTC July 21, 1994 (depicted in Figure 7) and its magnitude oscillated, until another maximum (180 W m^{-2}) of similar vertical distribution was realized at 0400 UTC on July 22. The heating at 2200 UTC seemed to be associated with a fossil (remaining part of diurnal solenoid over the form-

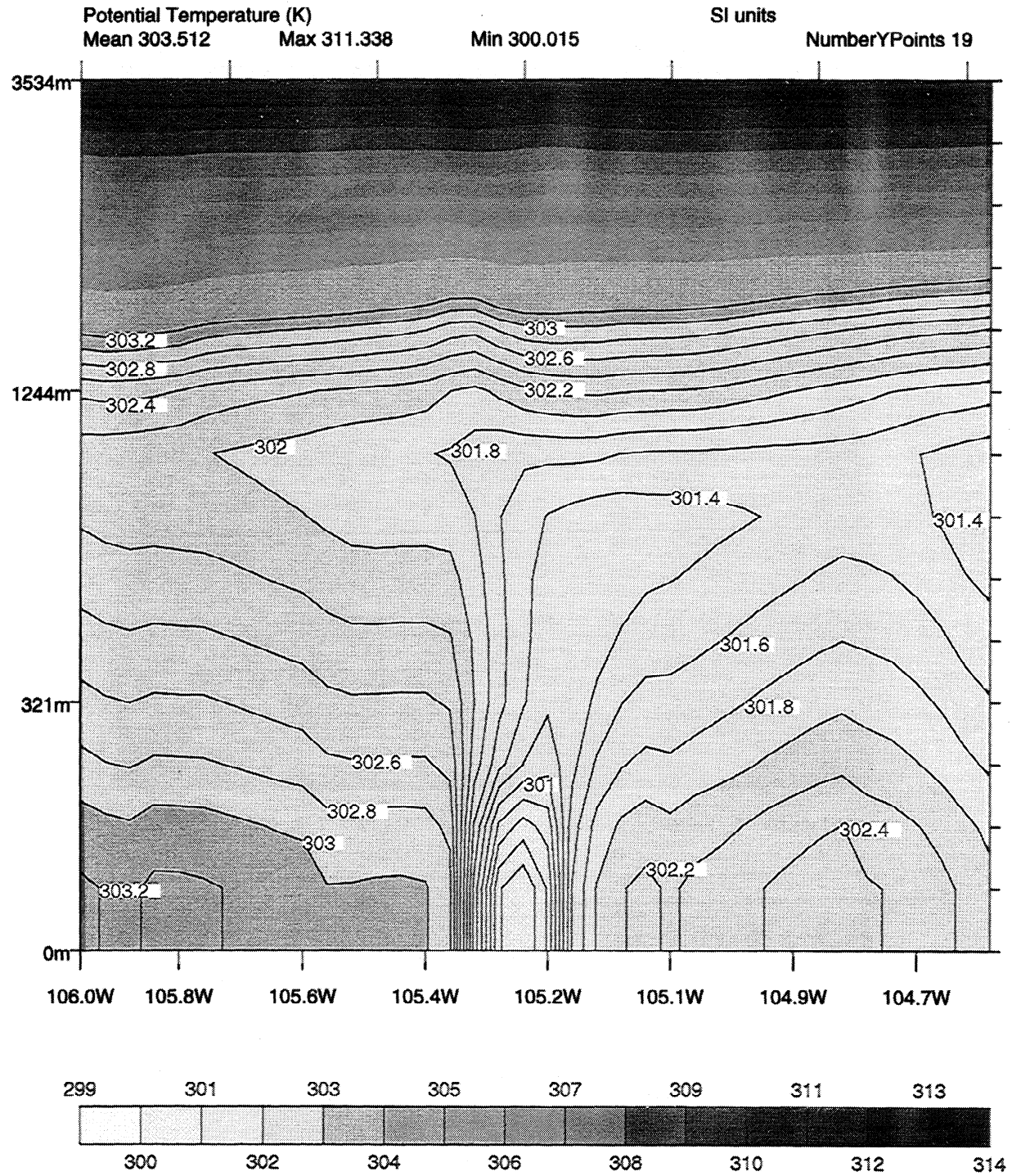

Figure 5. Modeled potential temperature profile over the aircraft transect for 1900 UTC, July 21, 1994. Contour interval of 0.2 K. Lakes are indicated by the contours near the surface and shown in Plate 1b. Reference lines are in decimal degrees.

ing nocturnal layer) uphill flow over the northern portion of Candle Lake and the NE slope, while the heating at 0400 UTC (Figure 8) could be associated with the downward export of colder air (from the nocturnal residual layer), when the two maxima in this field were located over the local orography minima and over Montreal Lake, where drainage flow and surface divergence were in place (see the winds in Plate 6). The mesoscale latent heat flux (not shown) had a maximum around 2200 UTC and a shorter lifetime. Most fields displayed SW to NE banding, which was a signature of the predominant westerly flow superposed on the local circulations caused by the orography.

By visually inspecting the grid 2 domain over many time periods, we found that the resolved fluxes contributed positively to the horizontally integrated heat budget of each model level over many hours and were observed to be horizontally displaced by the main flow. Vertically, we found these fluxes to be present exclusively within twice the depth of the diurnal

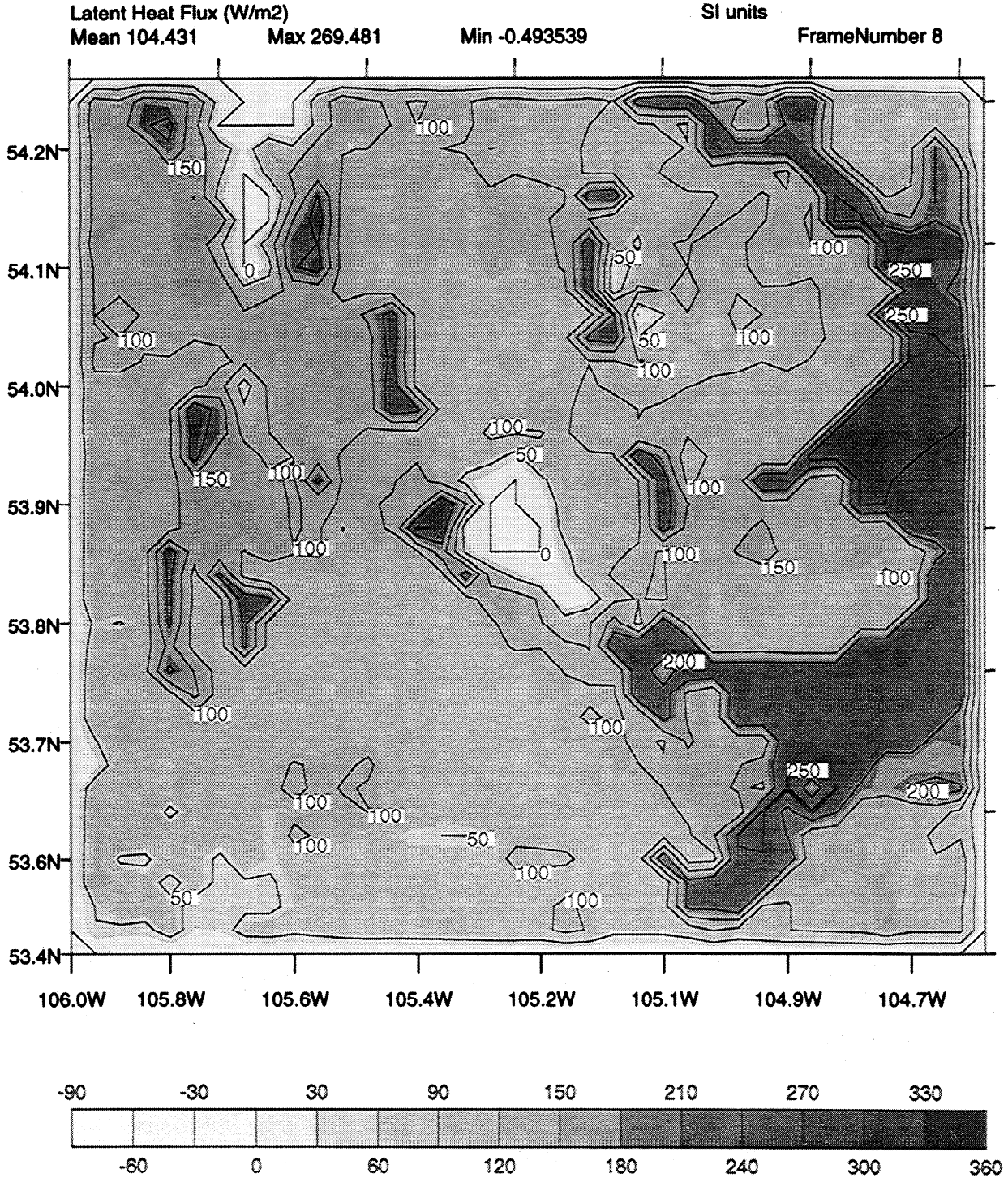

Figure 6. Fine-grid run: the grid 2 surface latent heat fluxes (W m^{-2}) at 1900 UTC, July 21, 1994. Contour interval of 50 W m^{-2}. Reference lines are in decimal degrees.

CBL. The magnitude of these fluxes for this case was indeed smaller than the magnitude of the surface turbulent fluxes, but their vertical distribution differed in that they peaked at higher levels, unlike the turbulent flux influence, which decays with height. Their accumulated impact is discussed in section 4.3.

In terms of timescales the mesoscale fluxes peaked about 3 hours after the realization of the maximum turbulent fluxes (1900 UTC), so that their phase lag was comparable with the timescale predicted by linear theory in section 3.1. Significant sensible heat fluxes persisted from 1800 UTC to about 0800 UTC between July 21 and 22, 1994.

4.2.4. Results for grid 3 (Δx = 625 m): the Candle Lake breeze. Grid 3 was spawned around Candle Lake with the purpose of resolving possible lake-induced circulations. After one full diurnal cycle, the model developed a well-defined lake breeze, identifiable in Figure 9 (depicting vertical velocity at 1250 m), with a subsiding cell (-0.286 m s^{-1}) to the NW of the lake center and maximum ascending motion (0.157 m s^{-1}) at

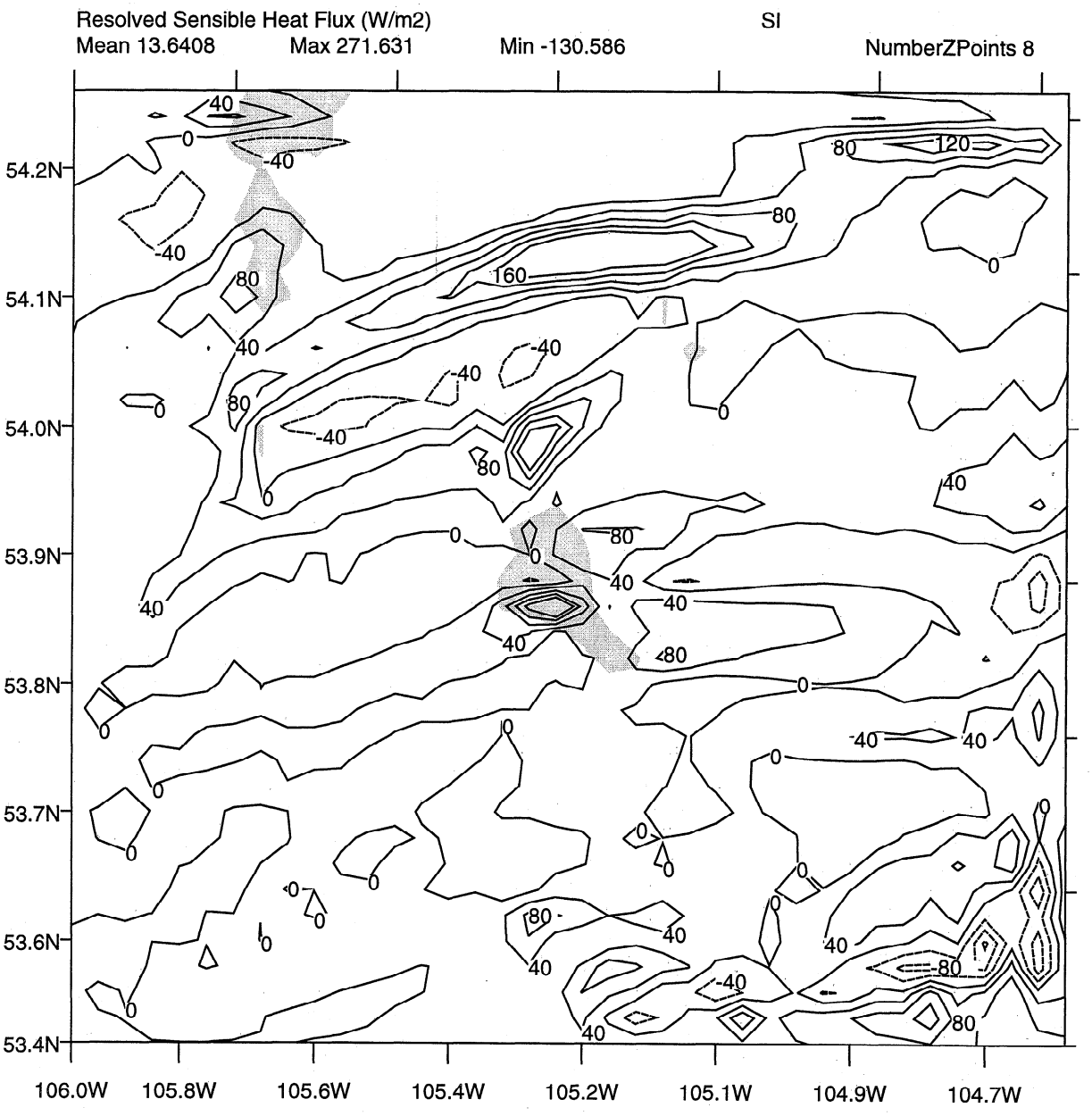

Figure 7. Fine-grid run: mesoscale (resolved) sensible heat flux (W m^{-2}) for grid 2, 2200 UTC, July 21, 1994, at 775 m. Contour interval of 40 W m^{-2}. Reference lines are in decimal degrees. Lakes are shown by light shading.

the northwest bank of the lake. The downward motion region revealed a shape and position that confirmed the influence of Candle Lake. The positive vertical velocity regions were distributed over the land around the lake, although shifted by the southwesterly winds.

A lake-induced circulation was also observed at night (22 July, 0600 UTC, Figure 10), with ascending motion (0.115 m s^{-1}) over the eastern part of the lake and descending motion (minimum of -0.104 m s^{-1}) over the western lake boundaries. Most of the ascending motion over the central part of the lake was shifted eastward by the prevailing winds.

This pattern of ascending/descending motion corresponds to a diurnal cycle in mass divergence over the lake. This pattern was observed on July 21 by three aircraft, as discussed previously, and is portrayed in Figure 4. During the diurnal heating period, with ascending motion over the lake boundaries and descending motion over the center of the lake, there was divergence at low levels near the lake center. During the nocturnal cooling period there was descending motion over the lake boundaries and ascending motion at low levels near the lake center, where the land breeze converged with the prevailing flow. A typical conceptual model for the Candle Lake circulation was also given by *Sun et al.* [this issue, Figure 3], which is consistent with our modeling results.

Superimposed on the lake breeze, the previous discussion of the wind fields pointed to contributions by the local orography (Candle Lake is positioned in a depression which slopes to the NE and NW with local terrain reliefs of 150 m within 50 km, which can control a coupled nocturnal surface flow converging at the lake center). The evidence of this influence on July 21

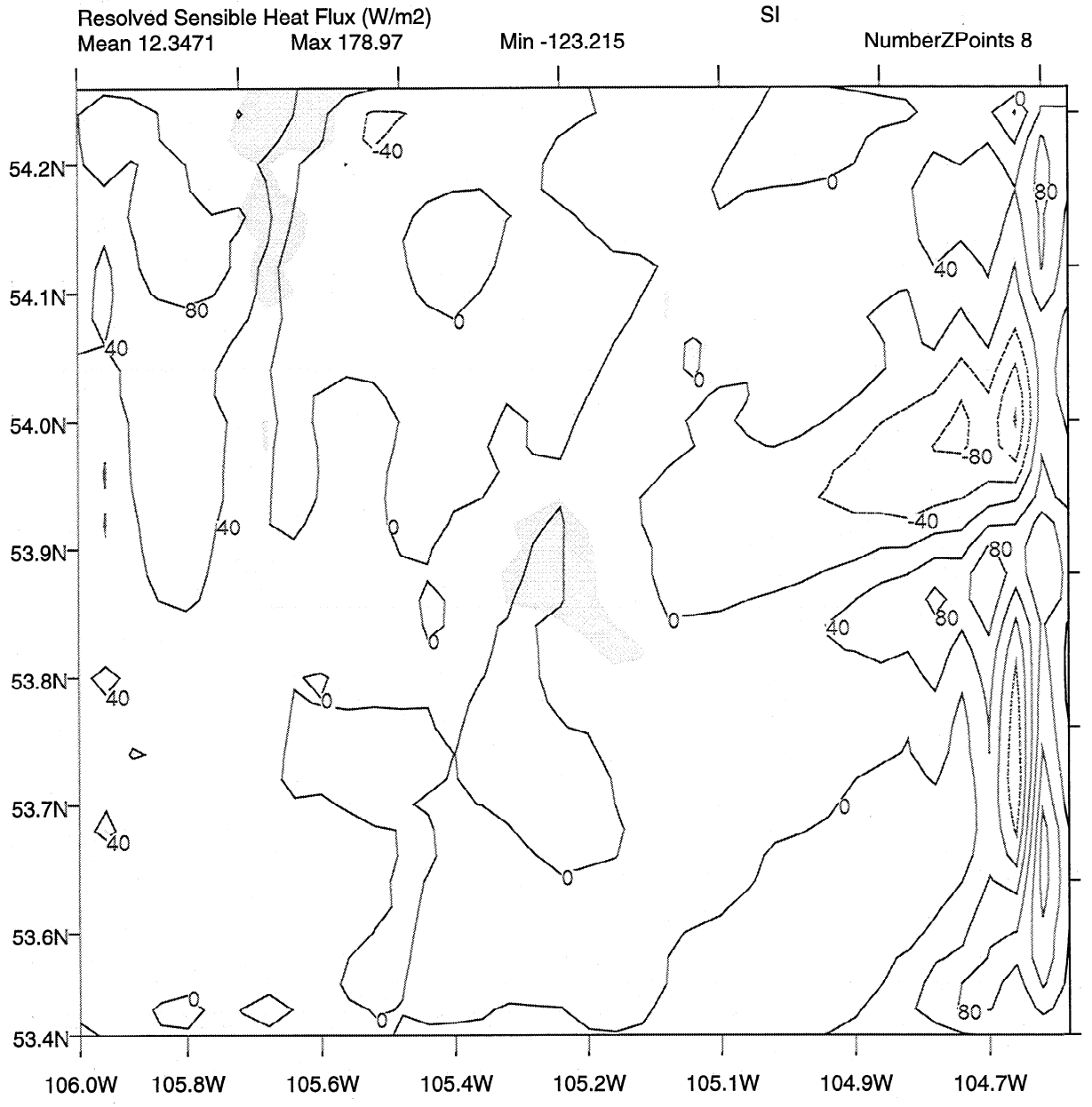

Figure 8. Fine-grid run: mesoscale (resolved) sensible heat flux (W m^{-2}) for grid 2, 0400 UTC, July 22, 1994, at 775 m. Contour interval of 40 W m^{-2}. Reference lines are in decimal degrees. Lakes are shown by light shading.

was present in Plates 5 and 6, which shows how the surface winds turned toward the SE (downslope) as the nocturnal cooling was initiated. The nocturnal land breeze displayed an ascending cell over the east bank of the lake, illustrating how the prevailing flow shifted the convergence zone toward the N-NE. Another indication of the occurrence of this enhanced nocturnal convergence at low levels is that the vertical velocity in the nocturnal ascending cell had a considerably larger areal extent than the one during the daylight. The issue of the local coupling of the lake breeze with a mountain-valley type circulation needs to be explored through simulations of days with lower synoptic scale winds.

4.3. Model Average Sounding and Diurnal Cycle Heating

The working hypothesis behind setting up a fine-grid run and a coarse-grid run over the grid 1 domain was that the coarse-grid run had truncated resolution and was not capable of effectively representing the full spectrum of mesoscale contributions (lacking both explicit and parameterized representation of mesoscale atmospheric processes with scales up to 40 km). We thus calculated horizontal averages of the vertical potential temperature (θ) profile for the region corresponding to grid 3 at every model output time (every 3600 s). The averages were taken over the exact same region in both the fine-grid and the coarse-grid runs. We then calculated a diurnal vertical heating curve by subtracting the horizontally averaged θ vertical profile at 23 UTC on 21 July from the horizontally averaged vertical θ profile at 1100 UTC on the same day. Because of the mesoscale time lag of 2 hours (as compared to turbulence) indicated by the analysis in section 3 and the results in section 4.2.3, later times would have been more revealing but would not have been suitable for comparison to the data from the

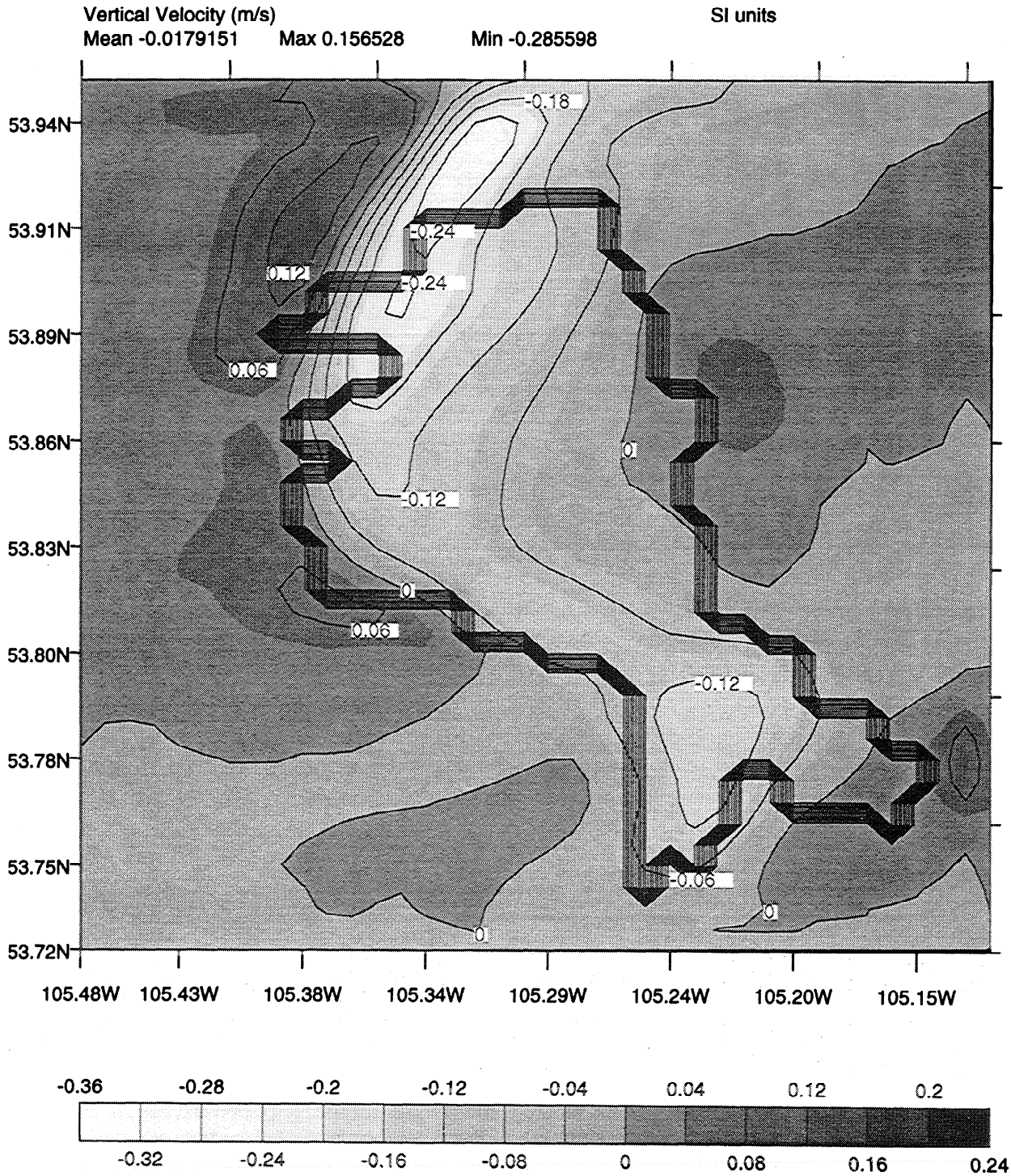

Figure 9. Fine-grid run: horizontal cross section of vertical velocity over Candle Lake for RAMS grid 3, 1800 UTC, July 21, 1994, at 250 m. Contour interval of 0.06 ms^{-1}. Reference lines are in decimal degrees.

soundings at the Candle Lake station (the last sounding was taken at 2300 UTC each day).

The results from our analysis are shown in Figure 11 and overall are in strong agreement with the findings of *Dalu et al.* [1996], particularly with their Figure 5d.

From comparison of the coarse-grid and the fine-grid diurnal heating patterns the coarse-grid run showed less vertically integrated heating than the fine-grid run, although displaying a comparable surface layer diurnal amplitude and cooling in the layer from 610 hPa to ~430 hPa. The diurnal profile in the fine-grid run showed more intense heating within the boundary layer and a cooling in the 550–390 hPa layer. The cooling above 280 hPa and the oscillations above the 570 hPa level are probably associated with vertical wave propagation [see also *Dalu et al.*, 1996, Figure 5d] and will be explored in an upcoming extension to the *Dalu et al.* [1996] analysis.

From the analysis in section 4.2.2 the near-surface turbulent sensible heat fluxes for the coarse-grid run were found, over

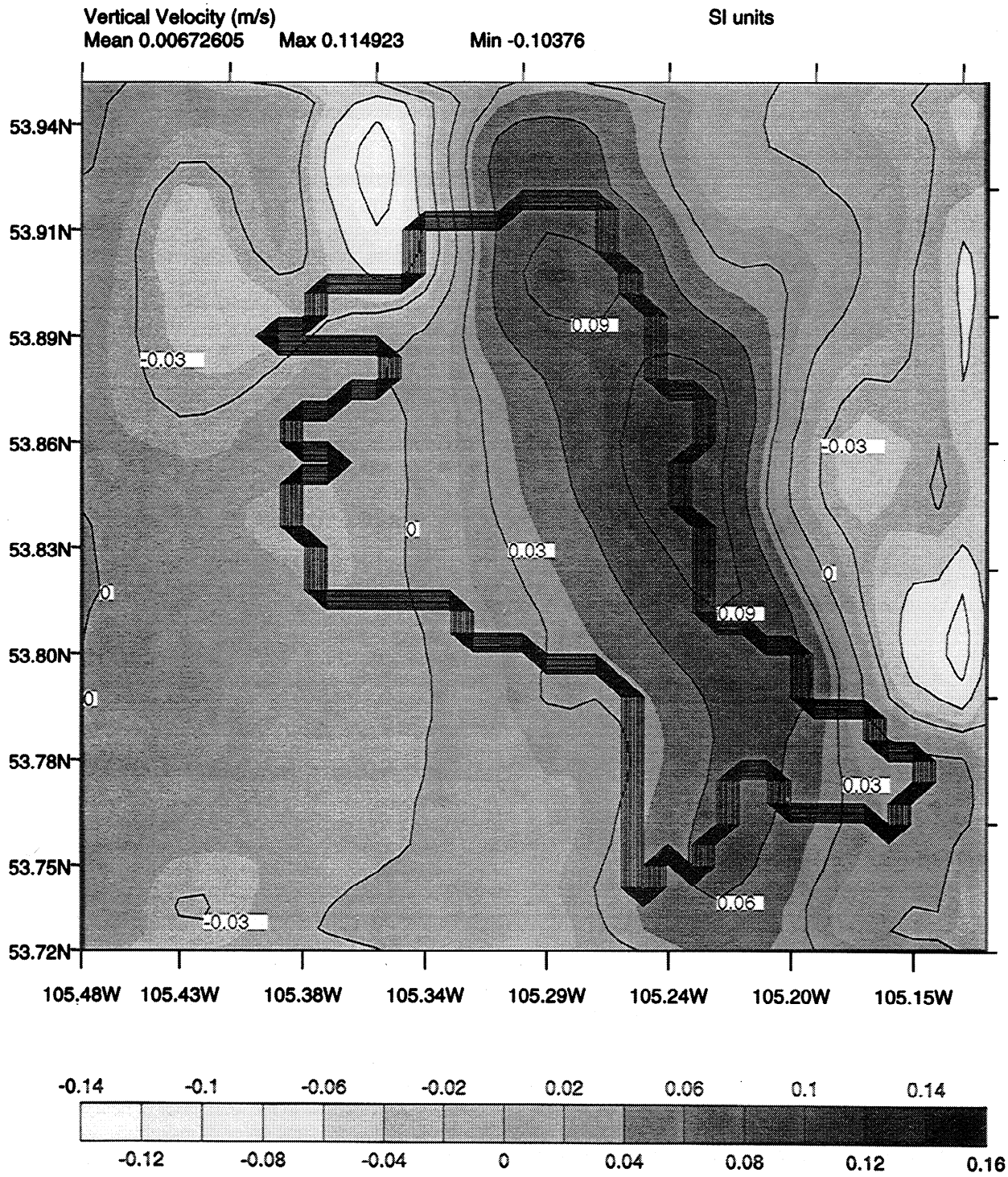

Figure 10. Fine-grid run: horizontal cross section of vertical velocity over Candle Lake for RAMS grid 3, 0600 UTC, July 22, 1994, at 250 m. Contour interval of 0.06 ms^{-1}. Reference lines are in decimal degrees.

the July 21 daytime, to be slightly less intense than those for the fine-grid run in the grid 3 model region. Our interpretation is that the coarse-grid run, although developing less intense surface sensible heat fluxes, lacked a secondary mechanism for the vertical redistribution of heat, thus developing a large surface temperature oscillation over the 12 hour period. The fine-grid run produced larger sensible heat fluxes at the surface but through resolved mesoscale circulations was capable of distributing this heat above the surface layer with more efficiency than if only parameterized turbulence had been active. Among the resolved circulations responsible for this vertical heat redistribution were the solenoidal circulations that we have shown to be active over the whole averaging period, i.e., the diurnal lake breeze and the nocturnal drainage flow and land breeze.

Data from the high-resolution (interpolated to 5 hPa) sounding at Candle Lake were used to calculate the 2317–1116 UTC (0516–1717 LT) temperature change on July 21, 1994,

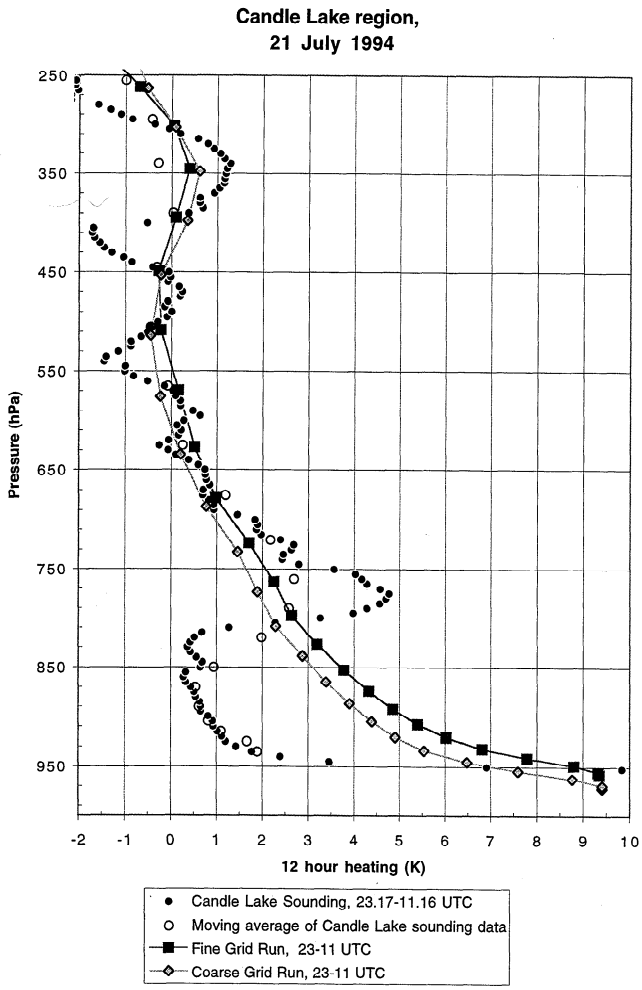

Figure 11. Horizontally averaged 12 hour temperature change over the RAMS grid 3 region for the coarse-grid and fine-grid runs between 1100 and 2300 UTC, on July 21, 1994. Candle Lake rawinsonde data for the period 1100 to 2300 UTC, on July 21, 1994, were used to calculate corresponding diurnal heating profiles. A vertical moving average of the rawinsonde data is overlaid (see text for explanation). Values are K per 12 hours.

and the resulting diurnal heating curve is shown on Figure 11. In order to help interpret the comparison, we have also provided a data set that was derived from the original sounding data by using a vertical moving average with a variable window width, which simulated the effect of vertical resolution in our atmospheric model. The variable window width is necessary since the model vertical grid is telescopic, with higher resolution at low levels; data at each point were therefore averaged over four vertical grid separations.

The comparison of the observed and simulated heating curves shows how the model was capable of reproducing the surface layer diurnal range with accuracy. The lower part of the boundary layer, however, heated too much in comparison to the observations, which is due in part to resolution and in part to the fact that the model temperature profiles are representative of an average over the grid 3 area but also to excessive vertical mixing. This can be confirmed by comparing the moving average profile with the model profiles and also by the fact that the model heating in the layer between 810 and 670 hPa is considerably less than the observed heating.

Further simulations with higher vertical resolution and a better specification of the BL vertical mixing coefficients are necessary to support this type of comparison; however, the performance of the model at other levels and the differences between the two simulations support our hypothesis.

5. Conclusions and Modeling Implications

We have analyzed information derived from remotely sensed data sets that were constructed for the BOREAS campaign, using the guidance of scaling criteria that were established through atmospheric dynamics principles. We have found that both the physiography and the surface heat fluxes do in fact exhibit organized patchiness that would be within the size interval necessary to generate mesoscale circulations.

The RAMS-LEAF-2 coupled model, heavily constrained with BOREAS data sets, was able to capture the surface turbulent flux variability across a portion of the BOREAS region with reasonable accuracy, without the need for special calibration. When this capability was established, the circulations generated by the model could be trusted to be representative of the local effects of the surface heterogeneity on the atmosphere. Using two distinct methods to simulate the contributions from the finer part of the surface heterogeneity, we found that the vertical distribution of the local heating generated by local mesoscale circulations agreed with the predictions of linear theory.

In conclusion, there is observational and modeling evidence to support the hypothesis that we cannot exclude contributions to large-scale heat fluxes by mesoscale wind circulations. The patchiness scales responsible for the generation of mesoscale circulations in the numerical model confirmed the usefulness of the scaling rules defined by the linear modeling study. These rules suggested that if the landscape heterogeneity is organized at spatial scales between twice the depth of the CBL and two local Rossby radiuses, mesoscale circulations should be either explicitly resolved or parameterized. The latter is probably the only present strategy available to large-scale modelers, because of computer power constraints; one such parameterization was proposed by *Zeng and Pielke* [1995a, b] and by *Pielke et al.* [1997].

Of course, it still remains to be determined whether the occurrence of mesoscale circulations displays significant climatological frequency, but the present analysis (as contrasted to linear analysis) seems to indicate that these circulations might even have significant impact on days with sustained synoptic winds. These effects seemed to manifest themselves in terms of mesoscale contributions to the total fluxes of heat which are, at their peak, about the same order of magnitude as the surface turbulent fluxes (in this case study, with sustained large-scale winds).

Modeled vertical temperature profiles for the region seemed to suggest the existence of a "signature" due to resolved transports of heat. The signature appeared as extra heating within and above the boundary layer as compared to cases in which the mesoscale circulations were hypothesized to be less active. The magnitude of the extra heating is on average (vertically) of 0.5 K per 12 hours over a depth of almost 5000 m.

The very heterogeneous and discontinuous nature of the BOREAS landscape reinforces the usefulness of regional atmospheric models as complex data integrators. The differences in simulated surface fluxes and their impact on the atmosphere indicate that the "mosaic" approach should be used with caution in regions where the landscape patchiness comprises

scales between twice the CBL depth and twice the local Rossby radius.

The regional BOREAS land cover classification proved adequate for the modeling presented in this paper, which is limited to a specific region at a specific time. This data set is supported by accessory data sets that complement it and make the specification of RAMS-LEAF-2 boundary conditions possible. However, numerous land management, fire history, and interannual variability issues certainly indicate that a remote sensing approach, directly providing fields of LAI, albedo, and roughness length, may, in general, be better suited to force the model.

For the future it would be useful, given the necessary computer power, to build a suite of modeling case studies illustrating the relationship between synoptic wind intensity and relative contributions of mesoscale and turbulent fluxes to the total budget of heat. It would also be desirable to run a season-long simulation at two different resolutions (one of coarse-grid type, one of the fine-grid type) in order to test both the impact of the definition of surface physiography and the impact of the truncation in atmospheric scales.

Acknowledgments. The work here described has been sponsored by the Brazilian Government (CAPES grant 1152-92) by the National Science Foundation (NSF grant ATM9306754), and by NASA (grant NAG 5-2302). The physiography data for assimilation in RAMS were obtained from the United States Geological Survey, under contracts 14-08-0001-A0929 and 1434-94-A-1275. We thank D. Baldocchi, T. Crawford, G. Dalu, L. Mahrt, S. Ogunemijo, P. Schuepp, and J. Sun for providing access to their data. We also wish to thank Dean Williams, PCMDI Software, Lawrence Livermore National Laboratory, who very kindly provided access to the VCS graphics package and technical assistance.

References

André, J.-C., P. Bougeault, J.-F. Mahfouf, P. Mascart, J. Noilhan, and J.-P. Pinty, Impact of forests on mesoscale meteorology, *Phil. Trans. R. Soc. London*, *324*, 407–422, 1989a.

André, J.-C., J. P. Goutorbe, T. Schmugge, and A. Perrier, HAPEX-MOBILHY: Results from a large-scale field experiment, in *Remote Sensing and Large-Scale Global Processes*, edited by A. Rango, pp. 13–20, Int. Assoc. of Hydrol. Sci., Wallingford, England, 1989b.

Avissar, R., and F. Chen, Development and analysis of prognostic equations for mesoscale kinetic energy and mesoscale (sub-grid-scale) fluxes for large-scale atmospheric models, *J. Atmos. Sci.*, *50*, 3751–3774, 1993.

Avissar, R., and R. A. Pielke, A parameterization of heterogeneous land surfaces for atmospheric numerical models and its impact on regional meteorology, *Mon. Weather Rev.*, *117*, 2113–2136, 1989.

Balling, R. C., Jr., The climatic impact of a Sonoran vegetation discontinuity, *Clim. Change*, *13*, 99–109, 1988.

Beljaars, A. C. M., and A. A. M. Holtslag, Flux parameterization over land surfaces for atmospheric models, *J. Appl. Meteorol.*, *30*, 327–341, 1991.

Betts, A. K., and A. C. M. Beljaars, Estimation of effective roughness length for heat and momentum from FIFE data, *Atmos. Res.*, *30*, 251–261, 1993.

Black, T. L., The new NMC mesoscale Eta model: Description and forecast examples, *Weather Forecasting*, *9*, 265–278, 1994.

Bolle, H.-J., et al., EFEDA: European Field Experiment in a desertification threatened area, *Ann. Geophys.*, *11*, 173–189, 1993.

Bonan, G. B., D. Pollard, and S. L. Thompson, Influence of sub-grid-scale heterogeneity in leaf area index, stomatal resistance, and soil moisture on grid-scale land-atmosphere interactions, *J. Clim.*, *6*, 1882–1897, 1993.

Chen, F., and R. Avissar, Impact of land-surface moisture variabilities on local shallow convective cumulus and precipitation in large-scale models, *J. Appl. Meteorol.*, *33*, 1382–1394, 1994.

Chen, J. M., and J. Cihlar, Retrieving leaf area index in boreal conifer forests using Landsat TM images, *Remote Sens. Environ.*, *55*, 153–162, 1996.

Clark, C. A., and R. W. Arritt, Numerical simulations of the effect of soil moisture and vegetation cover on the development of deep convection, *J. Appl. Meteorol.*, *34*, 2029–2045, 1995.

Claussen, M., Estimation of areally-averaged surface fluxes, *Boundary Layer Meteorol.*, *54*, 387–410, 1991.

Collins, D. C., and R. Avissar, An evaluation with the Fourier amplitude sensitivity test (FAST) of which land surface parameters are of greatest importance in atmospheric modeling, *J. Clim.*, *7*, 681–703, 1994.

Cotton, W. R., and R. A. Pielke, *Human Impacts on Weather and Climate*, 288 pp., Cambridge Univ. Press, New York, 1995.

Dalu, G. A., R. A. Pielke, R. Avissar, G. Kallos, M. Baldi, and A. Guerrini, Linear impact of thermal inhomogeneities on mesoscale atmospheric flow with zero synoptic wind, *Ann. Geophys.*, *9*, 641–647, 1991.

Dalu, G. A., R. A. Pielke, M. Baldi, and X. Zeng, Heat and momentum fluxes induced by thermal inhomogeneities, *J. Atmos. Sci.*, *53*, 3286–3302, 1996.

Davies, H. C., Limitations of some common lateral boundary schemes used in regional NWP models, *Mon. Weather Rev.*, *111*, 1002–1012, 1983.

Doran, J. C., and S. Zhong, Variations in mixed-layer depths arising from inhomogeneous surface conditions, *J. Clim.*, *8*, 1965–1973, 1995.

Doran, J. C., et al., The Boardman regional flux experiment, *Bull. Am. Meteorol. Soc.*, *73*, 1785–1795, 1992.

Doran, J. C., W. J. Shaw, and J. M. Hubbe, Boundary layer characteristics over areas of inhomogeneous surface fluxes, *J. Appl. Meteorol.*, *34*, 559–571, 1995.

Eastman, J. L., R. A. Pielke, and D. J. McDonald, Calibration of soil moisture for large eddy simulations over the FIFE area, *J. Atmos. Sci.*, in press, 1997.

Gash, J. H. C., and W. J. Shuttleworth, Tropical deforestation: Albedo and the surface-energy balance, *Clim. Change*, *19*, 123–133, 1991.

Gash, J. H. C., and C. C. Nobre, Climatic effects of Amazonian deforestation: Some results from ABRACOS, *Bull. Am. Meteorol. Soc.*, *78*, 823–830, 1997.

Gash, J. H. C., J. S. Wallace, C. R. Lloyd, A. J. Dolman, M. V. K. Sivakumar, and C. Renard, Measurements of evaporation from fallow Sahelian Savannah at the start of the dry season, *Q. J. R. Meteorol. Soc.*, *117*, 749–760, 1991.

Guo, Y., and P. H. Schuepp, An analysis of the effect of local heat advection on evaporation over wet and dry surface strips, *J. Clim.*, *7*, 641–652, 1994.

Haurwitz, B., Comments on the sea-breeze circulation, *J. Meteorol.*, *4*, 1–8, 1947.

Henderson-Sellers, A., Z.-L. Yang, and R. E. Dickinson, The project for intercomparison of land-surface parameterization schemes, *Bull. Am. Meteorol. Soc.*, *74*, 1335–1349, 1993.

Jarvis, P. G., The interpretation of the variation in leaf water potential and stomatal conductance found in canopies in the field, *Philos. Trans. R. Soc. London, Ser. B.*, *273*, 593–610, 1976.

Kosta, R. D., and M. J. Suarez, A comparative analysis of two land surface heterogeneity representations, *J. Clim.*, *5*, 1379–1390, 1992.

Lee, T. J., The impact of vegetation on the atmospheric boundary layer and convective storms, Ph.D. dissertation, 137 pp., Dep. of Atmos. Sci., Colo. State Univ., 1992.

Li, B., and R. Avissar, The impact of spatial variability of land-surface heat fluxes, *J. Clim.*, *7*, 527–537, 1994.

Louis, J. F., M. Tiedke, and J.-F. Geleyn, A short history of the PBL parameterization at the ECMWF, in *Workshop on Planetary Boundary Layer Parameterization*, pp. 59–80, Eur. Cent. for Medium-Range Forecasting, Reading, England, 1981.

Lynn, B. H., F. Abramopoulos, and R. Avissar, Using similarity theory to parameterize mesoscale heat fluxes generated by sub-grid-scale landscape discontinuities in GCMs, *J. Clim.*, *8*, 932–951, 1995.

Mahrt, L., Grid-averaged surface fluxes, *Mon. Weather Rev.*, *115*, 1550–1560, 1987.

Mahrt, L., and M. Ek, Spatial variability of turbulent fluxes and roughness lengths in HAPEX-MOBILHY, *Boundary Layer Meteorol.*, *65*, 381–400, 1993.

Mahrt, L., J. Sun, D. Vickers, J. I. MacPherson, and J. R. Pederson, Observations of fluxes and inland breezes over a heterogeneous surface, *J. Atmos. Sci.*, *51*, 2484–2499, 1994a.

Mahrt, L., J. I. McPherson, and R. Desjardins, Observations of fluxes

over heterogeneous surfaces, *Boundary Layer Meteorol.*, *67*, 345–367, 1994b.

Mahrt, L., J. Sun, J. I. MacPherson, N. O. Jensen, and R. Desjardins, Formulation of surface heat flux: Application to BOREAS, *J. Geophys. Res.*, this issue.

Manqian, M., and J. Jinjun, A coupled model on land-atmosphere interactions—Simulating the characteristics of the PBL over a heterogeneous surface, *Boundary Layer Meteorol.*, *66*, 247–264, 1993.

Mason, P. J., The formation of areally-averaged roughness lengths, *Q. J. R. Meteorol. Soc.*, *114*, 399–420, 1988.

Miller, N., Applications of a hierarchical systems flux scheme for interactively coupling subgrid land surface models with atmospheric models, *Tech. Rep. UCRL-JC-114100*, Univ. of Calif., Lawrence Livermore Natl. Lab., Livermore, Calif., 1993.

Nicholls, M. E., R. A. Pielke, J. L. Eastman, C. A. Finley, W. A. Lyons, C. J. Tremback, R. L. Walko, and W. R. Cotton, Applications of the RAMS numerical model to dispersion over urban areas, in *Wind Climate in Cities*, edited by J. E. Cermak et al., pp. 703–732, Kluwer Acad., Norwell, Mass., 1995.

Noilhan, J., J. C. André, P. Bougeault, J. Goutorbe, and P. Lacarrere, Some aspects of the HAPEX-MOBILHY programme: The data base and the modeling strategy, *Surv. Geophys.*, *12*, 31–61, 1991.

Ogunjemiyo, S., P. H. Schuepp, J. I. MacPherson, and R. L. Desjardins, Analysis of flux maps versus surface characteristics from Twin Otter grid flights in BOREAS 1994, *J. Geophys. Res.*, this issue.

Ookouchi, Y., M. Segal, R. C. Kessler, and R. A. Pielke, Evaluation of soil moisture effects on the generation and modification of mesoscale circulation, *Mon. Weather Rev.*, *117*, 2113–2136, 1984.

Ooyama, K. V., Conceptual evolution of the theory and modeling of tropical cyclone, *J. Meteorol. Soc. Jpn.*, *60*, 369–380, 1980.

Orlansky, I., A rational subdivision of scales for atmospheric processes, *Bull. Am. Meteorol. Soc.*, *56*, 527–530, 1975.

Pielke, R. A., *Mesoscale Meteorological Modeling*, 612 pp., Academic, San Diego, Calif., 1984.

Pielke, R. A., G. Dalu, J. S. Snook, T. J. Lee, and T. G. F. Kittel, Nonlinear influence of mesoscale land use on weather and climate, *J. Clim.*, *4*, 1053–1069, 1991.

Pielke, R. A., et al., A comprehensive meteorological modeling system—RAMS, *Meteorol. Atmos. Phys.*, *49*, 69–91, 1992.

Pielke, R. A., J. H. Rodriguez, J. L. Eastman, R. L. Walko, and R. A. Stocker, Influence of albedo variability in complex terrain on mesoscale systems, *J. Clim.*, *6*, 1798–1806, 1993.

Pielke, R. A., X. Zeng, T. J. Lee, and G. A. Dalu, Mesoscale fluxes over heterogeneous flat landscapes for use in larger scale models, *J. Hydrol.*, *190*, 317–336, 1997.

Pleim, J. E., and A. Xiu, Development and testing of a surface flux and planetary boundary layer model for application in mesoscale models, *J. Appl. Meteorol.*, *34*, 16–32, 1995.

Pitman, A. J., Assessing the sensitivity of a land-surface scheme to the parameter values using a single column model, *J. Clim.*, *7*, 1856–1869, 1994.

Raupach, M. R., Vegetation-atmosphere interaction in homogeneous and heterogeneous terrain: Some implications of mixed layer dynamics, in *Vegetation and Climate Interactions in Semiarid Regions*, edited by A. Henderson-Sellers and A. J. Pitman, pp. 105–120, Kluwer Acad., Norwell, Mass., 1991.

Schädler, G., N. Kalthoff, and F. Fiedler, Validation of a model for heat, mass, and momentum exchange over vegetated surfaces using LOTREX 10E/HIBE88 data, *Contrib. Atmos. Phys.*, *63*, 85–100, 1990.

Segal, M., and R. W. Arritt, Non-classical mesoscale circulations caused by surface sensible heat-flux gradients, *Bull. Am. Meteorol. Soc.*, *73*, 1593–1604, 1992.

Segal M., R. Avissar, M. C. McCumber, and R. A. Pielke, Evaluation of vegetation effects on the generation and modification of mesoscale circulations, *J. Atmos. Sci.*, *45*, 2268–2292, 1988.

Segal, M., W. Schreiber, G. Kallos, R. A. Pielke, J. R. Garratt, J. Weaver, A. Rodi, and J. Wilson, The impact of crop areas in northeast Colorado on midsummer mesoscale thermal circulations, *Mon. Weather Rev.*, *117*, 809–825, 1989.

Sellers, P. J., F. G. Hall, G. Asrar, D. E. Strebel, and R. E. Murphy, An overview of the First ISLSCP Field Experiment, *J. Geophys. Res.*, *97*, 18,455–18,466, 1992.

Sellers, P. J., et al., The Boreal Ecosystem-Atmosphere Study (BOREAS): An overview and early results from the 1994 field year, *Bull. Am. Meteorol. Soc.*, *76*, 1549–1577, 1995.

Shen, J., and R. W. Arritt, Comparison of GCM sub-grid fluxes calculated using BATS and SiB schemes with a coupled land-atmosphere high-resolution model, Preprints, paper presented at Seventh Symposium on Global Change Studies, Am. Meteorol. Soc., Atlanta, Ga., 28 January–2 February, 1996.

Shuttleworth, W. J., Daily variations of temperature and humidity within and above Amazonian forest, *Weather*, *40*, 102–108, 1985.

Simpson, J. E., *Sea Breeze and Local Wind*, 234 pp., Cambridge Univ. Press, New York, 1994.

Smith, E. A., et al., Area-averaged surface fluxes and their time-space variability over the FIFE experimental domain, *J. Geophys. Res.*, *97*, 18,599–18,622, 1992.

Steyaert, L. T., F. G. Hall, and T. R. Loveland, Land cover mapping, fire regeneration and scaling studies in the Canadian boreal forest with 1-km AVHRR and Landsat TM data, *J. Geophys. Res.*, this issue.

Sun, J., and L. Mahrt, Relationship of surface heat flux to microscale temperature variations: Applications to BOREAS, *Boundary Layer Meteorol.*, *76*, 291–301, 1995.

Sun, J., R. L. Desjardins, L. Mahrt, and J. I. MacPherson, The influence of lakes in the atmospheric transport of CO_2, water vapor and O_3 in BOREAS, in press, *J. Geophys. Res.*, 1997.

Sun, J., D. H. Lenschow, L. Mahrt, T. L. Crawford, K. J. Davis, S. P. Oncley, J. I. MacPherson, Q. Wang, R. J. Dobosy, and R. L. Desjardins, Lake-induced atmospheric circulations during BOREAS, *J. Geophys. Res.*, this issue.

Tremback, C. J., and R. Kessler, A surface temperature and moisture parameterization for use in mesoscale numerical models, Preprints, paper presented at the 7th Conference on Numerical Weather Prediction, Am. Meteorol. Soc., Montreal, 17–20 June 1985.

Wallace, J. S., I. R. Wright, and J. B. Stewart, The Sahelian Energy Balance Experiment (SEBEX): Ground based measurements and their potential for spatial extrapolation using satellite data, *Adv. Space Res.*, *11*, 131–142, 1991.

Wang, J., E. A. B. Eltahir, and R. L. Bras, 3D numerical simulation of mesoscale circulations forced by land surface thermal heterogeneities of random distribution, *J. Atmos. Sci.*, in press, 1997.

Wierenga, J., Roughness-dependent geographical interpolation of surface wind speed averages, *Q. J. R. Meteorol. Soc.*, *112*, 867–889, 1986.

Wood, E. F., D. P. Lettenmaier, and V. G. Zartarian, A land-surface hydrology parameterization with subgrid variability for general circulation models, *J. Geophys. Res.*, *97*, 2717–2728, 1992.

Wright, I. R., J. H. C. Gash, H. R. Da Rocha, W. J. Shuttleworth, C. A. Nobre, G. T. Maitelli, C. A. G. P. Zamparoni, and P. R. A. Carvalho, Dry season micrometeorology of central Amazonian ranch-land, *Q. J. R. Meteorol. Soc.*, *118*, 1083–1099, 1992.

Xian, Z., and R. A. Pielke, The effects of width of landmasses on the development of sea breezes, *J. Appl. Meteorol.*, *30*, 1280–1304, 1991.

Zeng, X., Chaos theory and its application in the atmosphere, *Atmos. Sci. Pap.*, 178 pp., *504*, Colo. State Univ., Boulder, 1992.

Zeng, X., and R. A. Pielke, Error-growth dynamics and predictability of surface thermally-induced atmospheric flow, *J. Atmos. Sci.*, *50*, 2817–2844, 1993.

Zeng, X., and R. A. Pielke, Further study on the predictability of landscape-induced atmospheric flow, *J. Atmos. Sci.*, *52*, 1680–1698, 1995a.

Zeng, X., and R. A. Pielke, Landscape-induced atmospheric flow and its parameterization in large-scale numerical models, *J. Clim.*, *8*, 1156–1177, 1995b.

Zhong, S., and J. C. Doran, A modeling study of the effects of inhomogeneous surface fluxes on boundary-layer properties, *J. Atmos. Sci.*, *52*, 3129–3142, 1995.

A. Barr, Atmospheric Environment Service, National Hydrology Research Centre, 11 Innovation Blvd., Saskatoon, SK, Canada S7N 3H5.

R. A. Pielke Sr. and P. L. Vidale, Department of Atmospheric Science, Colorado State University, Fort Collins, CO 80523. (e-mail: vidale@homebrew.atmos.colostate.edu)

L. T. Steyaert, U.S. Geological Survey, EROS Data Center, NASA Goddard Space Flight Center, Code 923, Building 22, Room G13, Greenbelt, MD 20771.

(Received April 29, 1996; revised September 9, 1997; accepted September 9, 1997.)